REPORT DOCUMENTATION PAGE

Form Approved OMB No. 0704-0188

1. REPORT DATE *(DD-MM-YYYY)*	2. REPORT TYPE	3. DATES COVERED *(From – To)*
05-01-2011	Final Report	1 November 2007 - 05 December 2010

4. TITLE AND SUBTITLE

Optical Parametric Fiber Oscillator and Amplifier for High Power, High Efficiency Operation at Around 0.8 microns

5a. CONTRACT NUMBER

FA8655-08-1-3013

5b. GRANT NUMBER

Grant 08-3013

5c. PROGRAM ELEMENT NUMBER

61102F

6. AUTHOR(S)

Professor Johan Nilsson

5d. PROJECT NUMBER

5d. TASK NUMBER

5e. WORK UNIT NUMBER

7. PERFORMING ORGANIZATION NAME(S) AND ADDRESS(ES)

University of Southampton
Highfield
Southampton SO17 1BJ
United Kingdom

8. PERFORMING ORGANIZATION REPORT NUMBER

N/A

9. SPONSORING/MONITORING AGENCY NAME(S) AND ADDRESS(ES)

EOARD
Unit 4515 BOX 14
APO AE 09421

10. SPONSOR/MONITOR'S ACRONYM(S)

AFRL/AFOSR/RSW (EOARD)

11. SPONSOR/MONITOR'S REPORT NUMBER(S)

Grant 08-3013

12. DISTRIBUTION/AVAILABILITY STATEMENT

Approved for public release; distribution is unlimited.

13. SUPPLEMENTARY NOTES

14. ABSTRACT

This report results from a contract tasking University of Southampton as follows.
Optical parametric fiber oscillators are based on four-wave mixing. Four-wave mixing (FWM), like stimulated Raman scattering (SRS), relies on the third order nonlinearity of the fiber. Fiber Raman devices are capable of high efficiency (> 80%) and high power (> 10 W), but these generate wavelengths that are longer than the pump wavelength. By contrast, FWM is capable of generating shorter wavelengths than the pump, and this provides many new opportunities, including the possibility to generate high-power 800 nm radiation starting with highly efficient YDFLs. Whereas SRS ideally generates one Stokes photon for every converted pump photon, FWM generates one Stokes and one anti-Stokes photon for every two pump photons. Thus, for small wavelength shifts, the conversion efficiency into the shorter-wavelength anti-Stokes wave is limited to ~ 50%. However, for larger shifts the efficiency can be larger. For generation of 780 nm light from 1080 nm, the theoretical photon-energy limited conversion efficiency becomes 69%, achievable if all pump photons are converted to anti-Stokes (signal) and Stokes (idler) photons. Complete conversion of the pump photons is theoretically possible in the cw regime [1] and near-complete conversion has been demonstrated experimentally in the cw regime [2], [3]. However the powers have been relatively low and the frequency shifts relatively small. Furthermore the wavelengths have been around 1550 nm.

15. SUBJECT TERMS

EOARD, Optical parametric oscillators, Fibre Lasers, Nonlinear Optics

16. SECURITY CLASSIFICATION OF:			17. LIMITATION OF ABSTRACT	18, NUMBER OF PAGES	19a. NAME OF RESPONSIBLE PERSON
a. REPORT	b. ABSTRACT	c. THIS PAGE			A. GAVRIELIDES
UNCLAS	UNCLAS	UNCLAS	SAR	31	19b. TELEPHONE NUMBER *(Include area code)* +44 (0)1895 616205

Progress Report

Fiber Optical Parametric Oscillator for High Power, High Efficiency Short-Wavelength Generation

5 December 2010

Grant: *FA8655-08-1-3013*
Authors: *Professor Johan Nilsson, Gysbert van der Westhuizen*
Address: *Optoelectronics Research Centre, University of Southampton, Southampton SO17 1BJ, UK*

1 Introduction

This report summarizes the work carried out at the Optoelectronics Research Centre over the period January 2009 to December 2010. The project involves the investigation of fiber-optical parametric amplifiers (OPA) and oscillators (OPO). Whereas the majority of work in this area has been conducted in the spectral region about 1550 nm, this project has explored the possibility of using ytterbium-doped fiber lasers (YDFL) and amplifiers (YDFA) as pump sources. The aim has been to obtain high power, high conversion efficiency devices, emitting at wavelengths in the transition region between the visible and near-IR parts of the spectrum. A specific objective has been to generate emission at 780-852 nm for Cs and Rb pumping. Experimentally, we demonstrated conversion to 715 nm. However, based on the dispersion characteristics of this fiber, generation at 780 nm should be possible by tuning the pump source to 1100 nm. A more general motivation for sources of this nature, is the fact that laser quality light is not readily available from conventional laser-technology at arbitrary wavelengths. The contents of this report details our experimental progress and builds on the groundwork of our initial report, for the period October 2007 to November 2008.

The following section offers a summary of our key findings. The interested reader are referred to Sections 3 through 5, for a more detailed discussion of the results.

2 Summary of findings

Experimental results

- Demonstrated fiber optical parametric oscillator (OPO) with 8.6% conversion efficiency to anti-Stokes at 715 nm.
    - *Record performance for any fiber OPO with frequency-shift over 140 THz.*
    - Used photonic crystal fiber (PCF) from *NKT Photonics*.
    - Anti-Stokes power reaches 170 mW at the PCF output end.
    - OPO cavity operated with 20% output-coupling.
- Low pump threshold of OPO allows for pumping with low-cost, power-scalable Yb-doped fiber master-oscillator power-amplifier (MOPA) with moderate peak output power.
    - Single-pass optical parametric generator (OPG) gave very low conversion at the corresponding power level, due to a much higher threshold.
    - Birefringent phase-matching in polarization maintaining (PM) fiber similarly failed in OPG configuration.

- Most aspects of fiber OPO well understood, but certain elements, like pulse-to-pulse fluctuations in the generated anti-Stokes, require further investigation.
- Parametric gain reduced by inefficient phase-matcing due to the the influence of longitudinal fiber variations.
- Reduced parametric gain exacerbated problems with competing nonlinear processes, such as stimulated Raman scattering (SRS).
  - Requires pump beam without the presence of seeding at the SRS wavelength.
  - Lack of fiber-coupled spectral filter precluded realization of all-fiber pump-OPO configuration.
- Observed strong pulse-pulse variations in generated anti-Stokes.
  - Degrades parametric conversion efficiency.
  - Suspected relation to polarization instabilities.
  - Possible relation to pump instabilities.
- Secondary SRS and other nonlinearities pumped by 715 nm anti-Stokes in 200 m long delay fiber reduced effective feedback.

Future work

- Realization of an all-fiber pump-OPO configuration.
  - Isolators with integrated special-purpose filters have been specified in conjunction with Shinkosha and can thus be purchased from them.
- Polarization-controlled cavity for improved efficiency.
  - PM feedback fiber.
  - PM WDM- and tap-couplers.
- More stable pump MOPA.
  - Diode seed source.
  - May lead to improved conversion efficiency.
- Mitigation of nonlinear effects in feedback fiber.
  - Use shorter feedback fiber. This will require a higher pump repetition frequency and therfore a higher average power.
  - Employ intra-cavity filters to reduce SRS build-up.
  - Reduce intra-cavity power by using higher output-coupling.
- Higher-power pump MOPA.
  - 3 W in all-fiber configuration and 10 W with free-space launch may be realistic in short-term.
- Longer-term, improved parametric fiber will lead to increased efficiency.
  - Dispersion engineering aimed at reducing PCF sensitivity to longitudinal fiber variations.
  - PM equivalents for greater stability.

Johan Nilsson
ORC, University of Southampton
Southampton, UK
jn@orc.soton.ac.uk
www.orc.soton.ac.uk
Phone: +44 23 8059 3101
Fax: +44 23 8059 3142
Mobile: +44 79 5753 6468

3 All-fiber Yb-based MOPA

One of the key benefits of a fiber OPA is the promise of all-fiber integration. From this point of view, an ytterbium-doped fiber-based pump source looks most attractive. Of particular interest is the master-oscillator power-amplifier (MOPA) configuration, which offers the control associated with a low-power seed laser, as well as the power scalability of double-cladding ytterbium-doped fiber amplifiers (YDFA).

The MOPA constructed for this work is shown in Figure 1. It consists of a CW fiber ring-laser centered at 1079 nm, externally modulated by an electro-optic modulator (EOM) before being amplified by three YDFAs. Polarization maintaining (PM) fiber is used throughout the MOPA to ensure single-polarization operation. To accommodate an all-fiber configuration, all three amplifiers are pumped through tapered fiber bundles. A narrowband (1 nm) tunable filter after the second amplifier helps to suppress the build-up of amplified spontaneous emission (ASE) and stimulated Raman scattering (SRS) in the final amplifier.

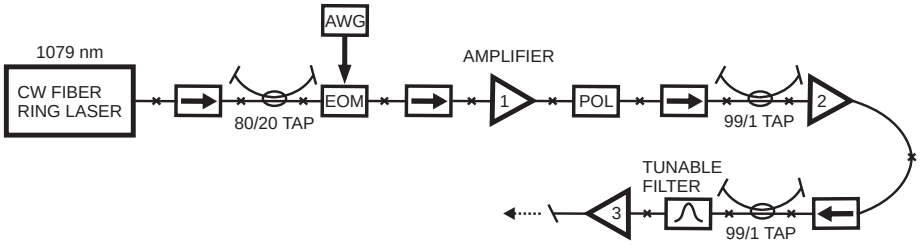

Figure 1: Schematic of a PM MOPA pump source, consisting of a CW fiber ring-laser, an electro-optic modulator (EOM), and three cascaded amplifier stages. (AWG: arbitrary waveform generator; POL: in-line polarizer).

Typical values for the pulse duration and repetition frequency (PRF) are 1 ns and 2 MHz, respectively. A pulse duration of 1 ns represents a good trade-off, since it is short enough to avoid stimulated Brillouin scattering (SBS), whilst being long enough to minimize walk-off, between the interacting waves, inside the nonlinear converter. The resulting peak power from the final amplifier is typically no more than 1 kW within the 40 pm linewidth at 1079 nm. This MOPA was used for most of our experiments, although other pump sources were tried as well.

4 Optical parametric generator

This section details our initial experimental investigations on optical parametric generation. The discussion summarizes aspects of the nonlinear fiber, that were chosen for the construction of a fiber OPG. Various results are briefly mentioned, with an emphasis on the underlying physical mechanisms.

4.1 Birefringence phase-matching

Birefringence phase-matching was investigated using a *Fujikura* SM98-PS-U25A PM fiber. This fiber uses stress-induced birefringence to maintain the polarization of a mode and is of the panda type. The dispersion and modal birefringence of this fiber was modeled using a commercial finite element method package (*Comsol*). The calculated modal birefringence of $B_m = 4.77 \times 10^{-4}$ at $\lambda = 1000$ nm was in good agreement with that obtained from a measurement of the beat length of this fiber ($B_m = \lambda / L_B = 4.84 \times 10^{-4}$). The resultant dispersion curve (for the slow fiber axis) is given in Figure 2(a) and shows a ZDW of approximately 1400 nm.

Depending on the polarization of the interacting waves, various phase-matching combinations are possible inside the *Fujikura* fiber [1, 2]. The phase matching combination that results in the largest frequency-shift requires both pump photons to be polarized along the slow fiber axis. The parametrically generated Stokes and anti-Stokes waves will then be polarized along the fast fiber axis. This process is illustrated in Figure 2(b), which shows the phase mismatch as a function of frequency-shift, for a pump wavelength of 1079 nm. Phase-matching occurs at a frequency-shift of roughly 78 THz, corresponding to a Stokes and anti-Stokes wavelength of 1503 nm and 841 nm, respectively.

Johan Nilsson
ORC, University of Southampton
Southampton, UK
jn@orc.soton.ac.uk
www.orc.soton.ac.uk
Phone: +44 23 8059 3101
Fax: +44 23 8059 3142
Mobile: +44 79 5753 6468

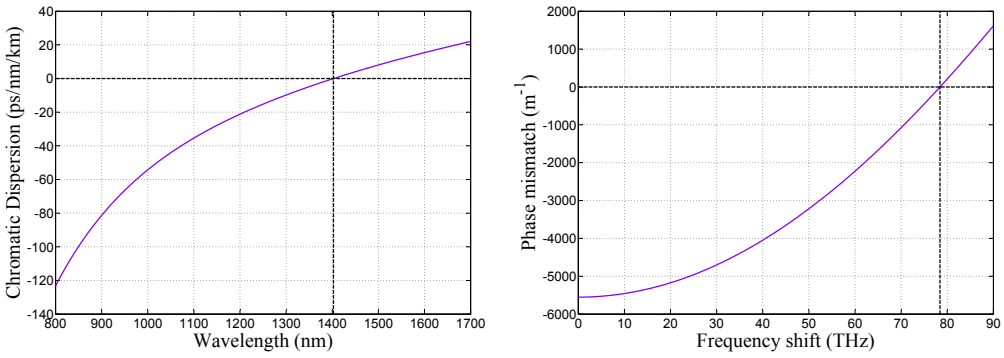

(a) (b)

Figure 2: (a) Chromatic dispersion of the *Fujikura* fiber. (b) Phase mismatch as a function of frequency shift for a pump wavelength of 1079 nm.

The procedure leading up to Figure 2(b) was repeated for a range of pump wavelengths, for two phase-matching processes. Figure 3(a) corresponds to the results of the preceding paragraph, where both pump photons are polarized along the slow fiber axis. In contrast, Figure 3(b) shows the case where both fiber polarizations are pumped. This allows for phase-matching with one pump photon in each polarization. This phase-matching combination reveals significantly smaller values for the frequency-shift and will result in a Stokes and anti-Stokes wave that is slow and fast-polarized, respectively.

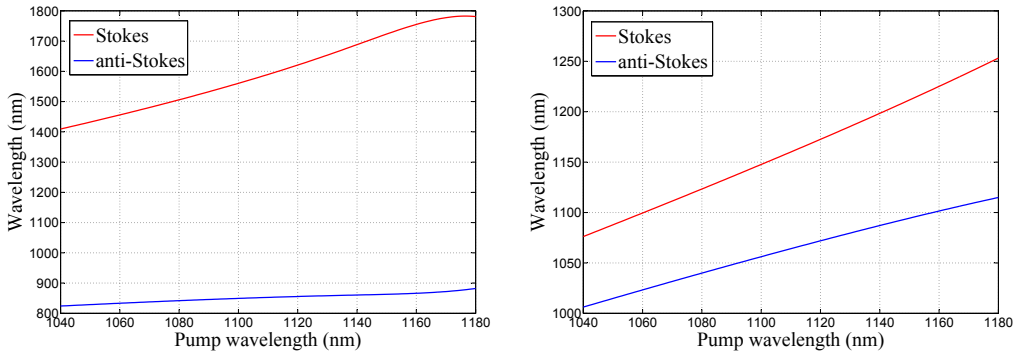

(a) (b)

Figure 3: Calculated phase-matching diagram for the *Fujikura* fiber for: (a) The case where the pump is polarized along the slow axis. (b) The case where both fiber polarizations are pumped.

4.2 Results

The output from the fiber MOPA of Figure 1 was lens-coupled into 21 m of *Fujikura* fiber. Free-space coupling was necessitated by the requirement for a spectral filter (in this case, a volume Bragg-grating (VBG)) to suppress seeding at SRS wavelengths. This is crucial, since the decreased FWM gain coefficient, associated with the interaction between orthogonally polarized waves, is comparable to the SRS gain coefficient. Effective FWM therefore requires spectral discrimination against SRS, which is not conditional on phase-matching.

The output spectrum of the nonlinear converter was measured with an optical spectrum analyzer (OSA). In the absence of seeding, the spectrum did not reveal any sign of parametric generation. However, upon seeding the parametric process with a CW source at 1490 nm, a corresponding anti-Stokes component was generated, in excellent agreement with Figure 3(a). The spectrum is shown in Figure 4(a) for a pump peak power of 190 W (1 ns pulses at a PRF of 5 MHz) and a seed power of 100 mW. Note that the pump wave in the spectrum is attenuated by approximately 20 dB, relative to the rest of the spectrum.

Johan Nilsson
ORC, University of Southampton
Southampton, UK
jn@orc.soton.ac.uk
www.orc.soton.ac.uk
Phone: +44 23 8059 3101
Fax: +44 23 8059 3142
Mobile: +44 79 5753 6468

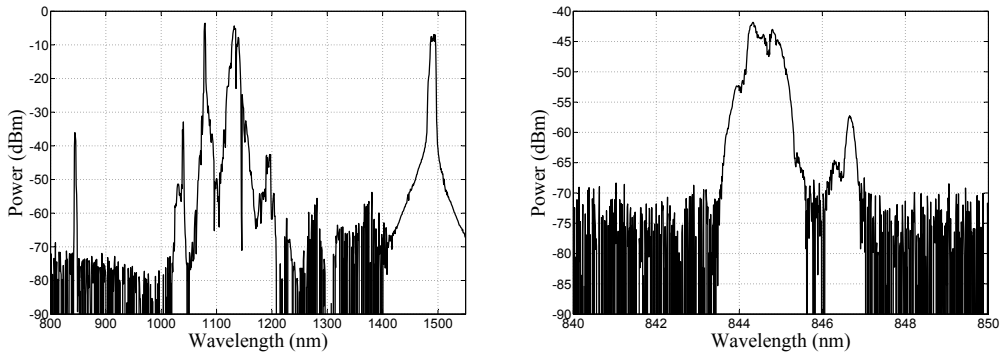

(a) (b)

Figure 4: (a) Output spectrum from 21 m of *Fujikura* fiber under CW seeding at the Stokes wavelength (spectral resolution is 2 nm). (b) High resolution spectrum of the generated anti-Stokes (spectral resolution is 0.1 nm).

Attempts at scaling the anti-Stokes power by scaling the pump power were unsuccessful, which we attribute to inadequate phase-matching. The presence of a strong Raman Stokes and associated Raman anti-Stokes is a further indication that the FWM process is subject to inadequate phase-matching. This theory is supported by a high-resolution spectrum of the generated anti-Stokes (Figure 4(b)). The anti-Stokes has a substructure consistent with the FWM spectrum that may be expected from a fiber that suffers from longitudinal inhomogeneity. Small changes in the waveguide dimensions will relate to a shift in the exact wavelengths for which phase-matching is achieved. Since the parametric bandwidth of the 78 THz frequency-shift FWM process is of the order of 0.01 nm [3], the new phase-matched wavelengths may well be outside of this bandwidth, which will result in a broadening of the anti-Stokes spectrum [4]. Similar experiments with shorter lengths of *Fujikura* fiber showed a narrowing of the generated anti-Stokes, which corroborates the preceding argument.

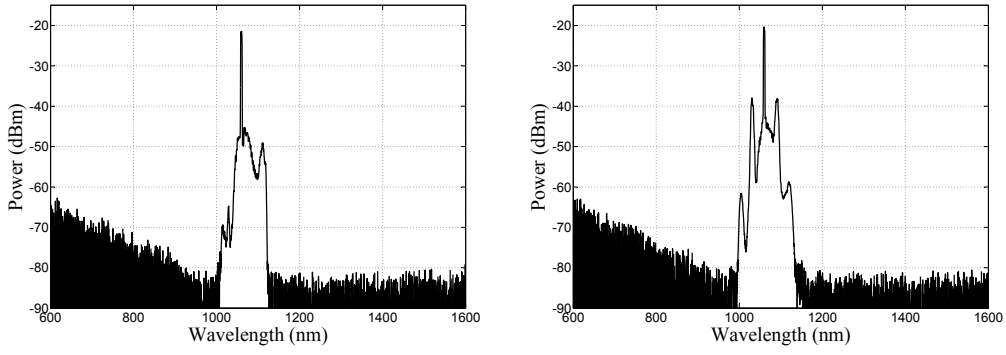

(a) (b)

Figure 5: Unseeded output spectra from 1 m of *Fujikura* fiber, using a high power picosecond pump source: (a) Input pump polarization aligned to the slow fiber-axis. (b) Input pump polarization optimized for small-shift FWM. In both cases, the spectral resolution is 1 nm.

In another experiment, a 1 m length of *Fujikura* fiber was pumped by ∼10 kW, 20 ps pulses at 1060 nm. The PM MOPA source for this experiment is detailed in Ref. [5]. At these power levels, the calculated parametric bandwidth for the large frequency-shift process approaches 0.5 nm. However, as a result of the large initial pump linewidth (∼0.4 nm), the effective length for FWM is severely limited by SPM-induced spectral broadening at 1060 nm. As a result, no parametric conversion was observed and the output spectrum was dominated by SRS (Figure 5(a)). This is in contrast to the case where the input pump polarization was aligned at 45°to the slow fiber-axis. Figure 5(b) shows strong parametric conversion to a Stokes wave at 1090 nm and an anti-Stokes wave at 1030 nm, which is in good agreement with Figure 3(b). This parametric process is characterized by a bandwidth of the order of 9 nm and is clearly dominant over the competing SRS process. As the pump power was further increased, pump saturation as a result of this small-shift FWM process was confirmed. The result therefore emphasized

Johan Nilsson
ORC, University of Southampton
Southampton, UK
jn@orc.soton.ac.uk
www.orc.soton.ac.uk
Phone: +44 23 8059 3101
Fax: +44 23 8059 3142
Mobile: +44 79 5753 6468

the importance of the parametric bandwidth and the requirement for a narrow linewidth high peak power pump source.

As our fiber MOPA in Figure 1 is limited in terms of the peak power it can deliver, a final experiment made use of a Nd:YAG pump laser at 1064 nm. The Nd:YAG laser has a linewidth of a few GHz and therefore offered the opportunity to investigate the *Fujikura* fiber in a different regime. The maximum pulse energy that was successfully coupled into 2 m of fiber was 53 μJ (10 ns pulses at a PRF of 10 Hz). Although the peak power of the pulse envelope only approached 3 kW, the pulse contained sharp features of width ∼100 ps and peak powers in the range 7 to 10 kW. The output spectrum, given in Figure 6, revealed the presence of noise-seeded parametric generation in addition to efficient SRS. The anti-Stokes once more showed a double-peak structure, although only one peak could be observed at the Stokes wavelength. The peak at 857 nm in the anti-Stokes spectrum may be a result of SRS, generated by the FWM anti-Stokes at 846 nm. Temporal analysis showed a correlation between the generated FWM pulses and the spikes in the pump pulses.

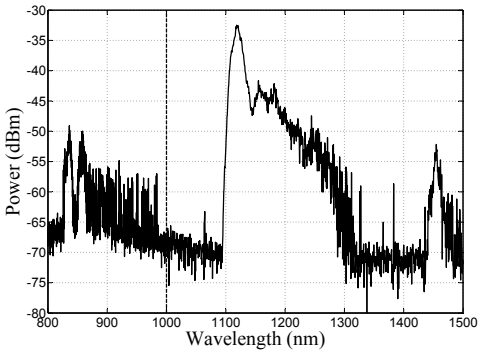

Figure 6: Unseeded output spectrum from 2 m of *Fujikura* fiber, using a narrow linewidth high energy Nd:YAG pump source. (spectral resolution is 2 nm).

5 PCF-based optical parametric oscillator

Although our results for the *Fujikura* fiber illustrated its potential use as an OPA, the conversion efficiencies were extremely low. We attribute this primarily to longitudinal fluctuations in the fiber diameter and the resulting dominance of competing SRS. It therefore became necessary to consider alternative methods to achieve phase-matching. To this end, we considered photonic crystal fibers (PCF) [6].

The airholes in the cladding of a PCF allow unprecedented customization of the fiber's dispersion through appropriate design. It is therefore possible to shift the ZDW to values below the ∼1300 nm limit that applies to conventional silica step-index fibers (see Section 4.1). In this way, it has been shown that large frequency-shift FWM can be achieved by pumping in the PCF's normal dispersion regime [7]. In fact, recent results have shown that this method of phase-matching can lead to exceptional parametric conversion efficiencies over frequency-shifts exceeding 100 THz [8, 9, 10].

This section is dedicated to our latest findings on PCF-based optical parametric devices. The PCF gain medium will be discussed in terms of its phase-matching properties, before we present results on an optical parametric oscillator. We will conclude with a discussion about the limitations of our current set-up and a comparison to the state-of-art in this field.

5.1 Fundamental-mode phase matching

After considering a number of PCFs, a large mode-area fiber from *NKT Photonics* was decided on. This fiber, labeled *PCF-LMA-8*, is characterized by $\Lambda = 5.6$ μm and $d/\Lambda = 0.49$ (Λ and d are the pitch and diameter of the PCF airholes, respectively). The dispersion for the PCF was once more calculated using *Comsol*. The result is shown in Figure 7(a) and yields a ZDW of 1153 nm. The dispersion data was then used to calculate the phase mismatch. In contrast to the *Fujikura* fiber, the nonlinear contribution is essential for the calculation of the phase mismatch in the PCF. This is due to the fact that the linear

Johan Nilsson
ORC, University of Southampton
Southampton, UK
jn@orc.soton.ac.uk
www.orc.soton.ac.uk
Phone: +44 23 8059 3101
Fax: +44 23 8059 3142
Mobile: +44 79 5753 6468

contribution to the phase mismatch converges to zero as the pump wavelength approaches the ZDW. The phase-mismatch was therefore calculated for a typical pump peak power of 1 kW. Figure 7(b) shows the phase mismatch as a function of frequency-shift for a pump wavelength of 1079 nm. Phase-matching is predicted at a frequency-shift of ∼132 THz. The phase-matched wavelengths as a function of the pump wavelength are given in Figure 7(c). This phase-matching diagram contrasts the frequency-shifts with pumping in the normal and anomalous dispersion regime and emphasizes the significance of the zero-dispersion wavelength for fiber FWM.

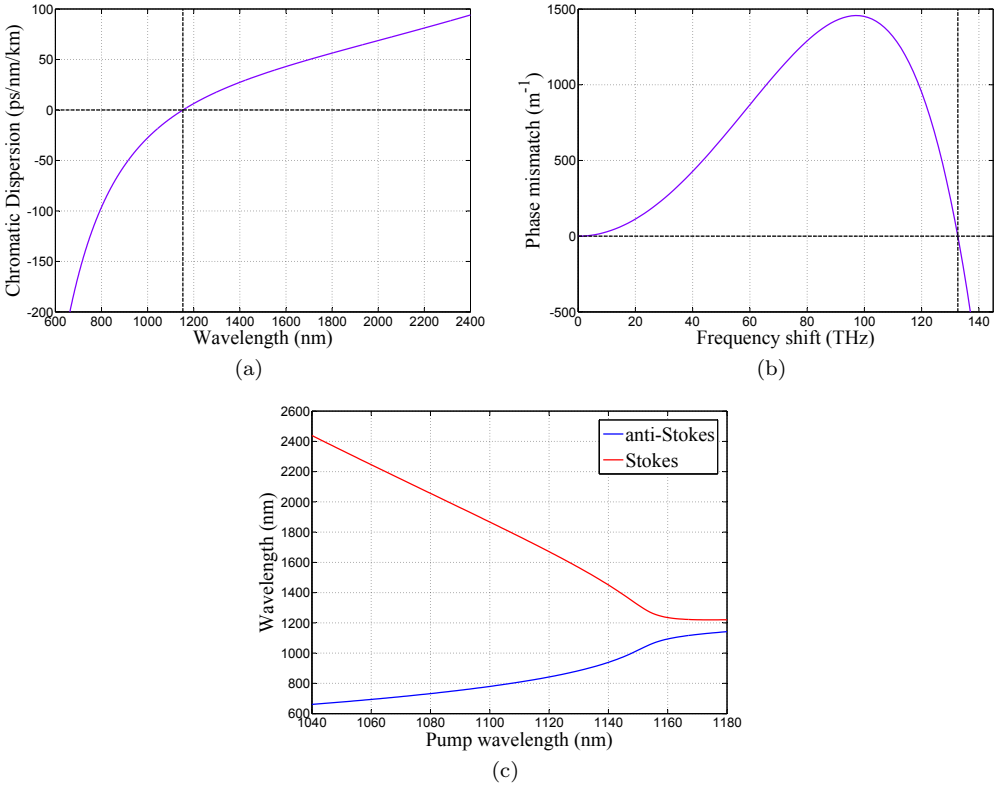

Figure 7: (a) Chromatic dispersion of the *PCF-LMA-8*. (b) Phase mismatch as a function of frequency shift for a pump wavelength of 1079 nm. (c) Calculated phase-matching diagram at a pump peak power of 1 kW.

One attractive property of this PCF is that it exhibits single-mode operation over the full wavelength range of interest (600 - 2500 nm). Particularly attractive is that the mode-field diameter, and consequently the effective mode-area, remains approximately constant. This improves the FWM conversion efficiency, since it ensures almost perfect spatial overlap between the interacting modes. Another property of large mode-area PCFs is that they are relatively insensitive against longitudinal inhomogeneity, compared to highly-nonlinear PCF varieties [10].

5.2 Results

The output of the fiber MOPA (Figure 1) was spliced directly to 18 m of *PCF-LMA-8*, operating as an OPG. The MOPA output was modulated with 1 ns pulses and a PRF of 1 MHz, resulting in a maximum PCF input peak power of 3 kW. The PCF output spectrum is given in Figure 8 and displays a supercontinuum (SC) stretching from 615 nm to beyond the long-wavelength limit of the spectrum analyzer (1750 nm). In addition to the pump wave and Raman Stokes at 1079 nm and 1131 nm, respectively, an anti-Stokes wave at 715 nm (142 THz frequency-shift) can clearly be identified. This value is not in perfect agreement with Figure 7(c), which predicts parametric sidebands at 730 nm and 2066 nm. The discrepancy may well be due to small differences in the specified and actual values for

Johan Nilsson
ORC, University of Southampton
Southampton, UK
jn@orc.soton.ac.uk
www.orc.soton.ac.uk
Phone: +44 23 8059 3101
Fax: +44 23 8059 3142
Mobile: +44 79 5753 6468

the structural parameters of the PCF. With the available equipment we were not able to measure the spectrum out to the Stokes wavelength.

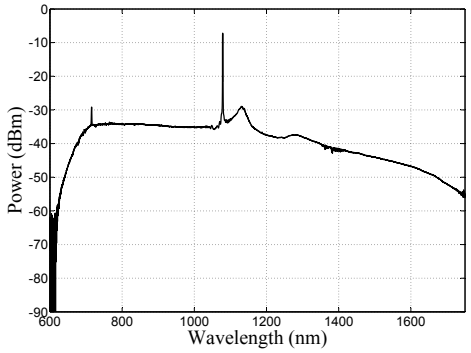

Figure 8: SC generated in the *PCF-LMA-8* in OPG configuration at a pump peak power of 3 kW. The spectrum shows a sharp feature at 715 nm, together with features at the pump (1079 nm) and Raman Stokes (1131 nm) wavelengths. The OSA spectral resolution is 1 nm.

Figure 8 again emphasizes the importance of discriminating against competing nonlinear processes. As the first order Raman Stokes cascades to higher orders that are located in the anomalous dispersion regime, the spectrum broadens rapidly as it propagates down the fiber. Therefore, the use of a spectral filter to reject SRS from the pump MOPA, and consequently a free-space launch, was once again required. Apart from seeding competing processes in the PCF, nonlinearities in the MOPA also presents a limitation to the peak power that it can deliver. Since the optical parametric oscillator (OPO) has been demonstrated as a means of lowering the parametric threshold [7], and thereby the power requirements for FWM, it was decided to reconfigure the PCF into a cavity [11].

Figure 9 shows the details of the OPO setup. The MOPA output is passed through a free-space isolator, before being diffracted by a volume Bragg-grating (VBG) with a bandwidth of ∼0.5 nm centered at 1079 nm. The VBG provides excellent extinction (≥30 dB) of all other spectral features. For partial polarization control, a half-wave plate is used to rotate the polarization angle of the linearly polarized MOPA output, before it is launched into the OPO cavity. Both ends of the PCF are spliced to a WDM-coupler (*Corning* Hi1060 fiber), to either combine or separate, the pump wave at 1079 nm and the anti-Stokes at its established wavelength of 715 nm. A delay line, consisting of 203 m of Hi1060 fiber, ensures that the round-trip time of the OPO cavity can be matched to the pump's PRF for synchronous pumping. Two cascaded 10% tap-couplers are used to extract 715 nm light from the cavity.

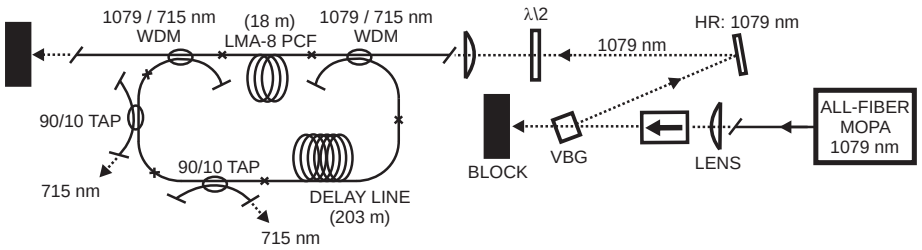

Figure 9: Schematic of the all-fiber cavity OPO. A volume Bragg-grating (VBG) is used as a spectral filter to remove unwanted seed-light at SRS wavelengths. WDM couplers are used to couple light into and out of the cavity. Two tap-couplers remove a total of 19% of the anti-Stokes radiation from the oscillator.

The cavity round-trip loss, dominated by PCF splice-loss and fiber loss in the delay line, was estimated to 6 dB. Additional loss was likely incurred at the input-WDM-coupler as a result of the anti-Stokes wavelength being below the single-mode cut-off wavelength of the Hi1060 fiber. Pump light was launched into the OPO via the input-WDM-coupler, which resulted in Raman scattering. In order to keep the SRS seeding at the PCF input to a minimum, the WDM pigtails were as short as possible. The MOPA was then operated at a PRF corresponding to half the round-trip time of the cavity. Precise

Johan Nilsson
ORC, University of Southampton
Southampton, UK
jn@orc.soton.ac.uk
www.orc.soton.ac.uk
Phone: +44 23 8059 3101
Fax: +44 23 8059 3142
Mobile: +44 79 5753 6468

synchronization to the cavity round-trip time was achieved by scanning the PRF of the MOPA, whilst monitoring the OPO output on an OSA. The resonant PRF had a value of 1.73 MHz.

The OPO output, as measured from the first tap-coupler, is given in Figure 10 for the cases with and without synchronized feedback. The corresponding pump peak power at the PCF input is 0.45 kW. In the absence of feedback, there is considerable SRS, but the SC seen in Figure 8 is absent. Although an anti-Stokes peak at 715 nm can be identified, it is very weak. Synchronization of the feedback changes this drastically, with the anti-Stokes peak growing by over 53 dB. The anti-Stokes wave has a linewidth of ∼0.8 nm (0.1 nm OSA resolution) and is accompanied by several Raman Stokes orders in the wavelength range 730-830 nm. The generated SRS is pumped by the FWM anti-Stokes as the waves propagate through the delay line fiber. In addition to the desired FWM, two peaks about the 1079 nm pump wavelength, at a frequency-shift of 2.6 THz, can be identified. Since these features show a dependence on the input pump polarization angle, they are thought to derive from accidental FWM due to birefringence phase-matching in the WDM-pitails. The long-wavelength edge of the spectrum in Figure 10 remains unchanged as the PCF input pump power is increased. This is due to the large bending loss of the tap-coupler pigtails (*Nufern* HP-780) at wavelengths longer than 1200 nm. Since the resultant loss for the FWM Stokes is very high, the tap-coupler effectively ensures that the OPO is singly-resonant [12].

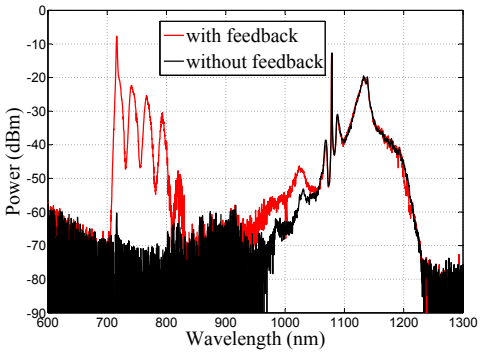

Figure 10: All-fiber cavity OPO output spectrum, measured from the first tap-coupler, in the absence (black), and presence (red) of synchronized feedback at a pump peak power of 0.45 kW. Synchronization is achieved at a MOPA PRF of 1.73 MHz, corresponding to half the cavity round-trip time. The anti-Stokes generates several orders of Raman Stokes in the delay line fiber. The OSA spectral resolution is 1 nm. Note that the WDM coupler attenuates wavelengths around the pump relative to those around the anti-stokes.

The use of cascaded tap-couplers resulted in strong attenuation at both 1079 nm and 1131 nm, as seen from Figure 11(a). It was therefore possible to measure the average power, contained at the anti-Stokes and its associated Raman orders, directly from the second tap-coupler, using a thermal power meter with a flat spectral response. This power is shown in Figure 11(b) as a function of input pump peak power. The threshold pump power is 0.41 kW. At a pump power of 0.45 kW, the second tap-coupler output power is 0.6 mW. From the coupling ratio, the anti-Stokes output from both couplers is 1.27 mW, whilst the corresponding power entering the delay line is 5.4 mW. This value is attenuated by an estimated 3.5 dB prior to reaching the PCF input, at which point the peak anti-Stokes seed power should be ∼1.39 W. The seed power therefore increases by approximately 69 dB, relative to the vacuum noise-level anti-Stokes seed power in the absence of feedback. This can be compared with the ∼53 dB increase in anti-Stokes power of Figure 10. The reason for this discrepancy is currently under investigation. One possibility is linewidth broadening in the feedback fiber. The SRS of the anti-Stokes in the feedback power also reduces the effective feedback.

The anti-Stokes power reaches 10.8 mW at a maximum pump power of 1.14 kW. The associated total anti-Stokes output power from both couplers is 22.8 mW, which translates to 170 mW at the PCF output. We can therefore deduce that the PCF converts 8.6% of the pump input power to anti-Stokes power.

Johan Nilsson
ORC, University of Southampton
Southampton, UK
jn@orc.soton.ac.uk
www.orc.soton.ac.uk
Phone: +44 23 8059 3101
Fax: +44 23 8059 3142
Mobile: +44 79 5753 6468

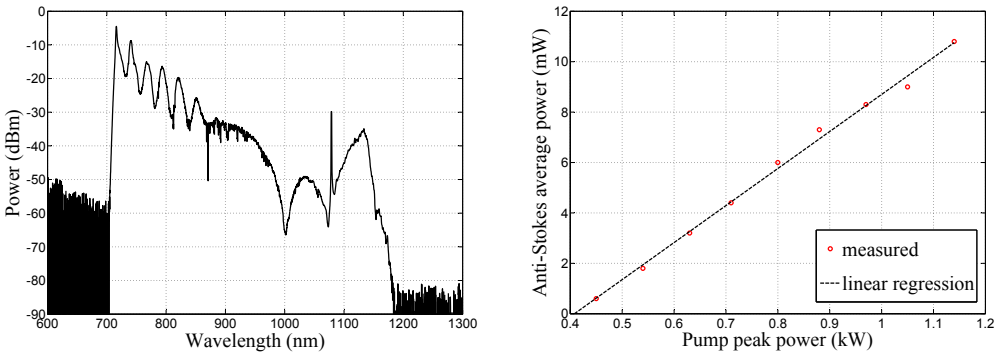

(a) (b)

Figure 11: (a) OPO output spectrum at a pump peak power of 1.14 kW, as measured from the second tap-coupler (spectral resolution is 1 nm). (b) Second tap-coupler output power as a function of pump peak power.

5.3 Discussion

Although 8.6% is a respectable conversion efficiency, it is still below what has been demonstrated in parametric oscillators with smaller wavelength shifts [13]. It is also smaller than the Raman conversion efficiency to 1132 nm, despite the intrinsically larger gain and smaller polarization dependence of the parametric process [2]. As was the case with the *Fujikura* fiber, inadequate phase-matching is a likely explanation for this. The calculated parametric bandwidth has a value of 60 pm for a pump power of 0.45 kW. This means that the measured anti-Stokes linewidth is more than an order of magnitude larger than the theoretical prediction. Since the MOPA linewidth is narrower than the pump acceptance bandwidth imposed by the calculated parametric bandwidth, longitudinal non-uniformity in the PCF is a likely reason for this [4]. Using the calculated dispersion of the PCF, the walk-off length of the three relevant waves can be calculated with respect to each other for a pulse duration of 1 ns [14]. The walk-off between the pump and the Stokes is the fastest and occurs over 21 m. This length, which exceeds that of the fiber, represents the distance over which FWM should dominate over competing nonlinear processes. However, the OPO spectrum in Figure 11(a), measured at the maximum pump power of 1.14 kW, still shows traces of a SC. The fact that FWM is unable to dominate over SRS, and the subsequent SC generation, supports the argument that inhomogeneities are degrading the OPO performance and points to a scenario where only short, and perhaps randomly distributed, fiber segments are contributing to the overall conversion [15].

The OPO output spectra gives clear evidence that the FWM anti-Stokes is being depleted by the Raman scattering generated in the delay line fiber. Using a delay line length of 75 m, the preceding experiment was repeated. The MOPA PRF was synchronized to the cavity round-trip time at a value of 1.95 MHz. The results did not reveal any significant changes in terms of threshold or conversion efficiency, but showed a decreased gain for the higher-order Raman Stokes-waves in the wavelength range 780 - 900 nm. Although a further decrease in delay fiber length will result in increased power scalability, the mechanism of synchronous pumping will require a corresponding increase in pump PRF. A higher PRF effectively means higher average power as a result of the OPOs inherent peak power demands. Since higher average powers lead to complications when it comes to the availability and price of fiberized components, alternative methods for power scaling must be considered. One alternative would be to decrease the power in the delay fiber by using a higher output-coupling ratio. This method will increase the cavity round-trip loss and will lead to a higher pump threshold power. However, the increase in threshold may well be acceptable in terms of the available pump power.

In an attempt to increase the parametric bandwidth to study the influence of fiber inhomogeneity, an OPO was also constructed using a 2 m length of *PCF-LMA-8*. According to calculations, this length would be sufficient to generate the parametric gain and conversion corresponding to Figure 11(b). However, we were not able to detect any conversion. Furthermore, an investigation into the temporal behavior of the output from the OPO, using 18 m of PCF, revealed that not every pump pulse is converted into a corresponding anti-Stokes pulse. Although variations along the length of the fiber are

Johan Nilsson
ORC, University of Southampton
Southampton, UK
jn@orc.soton.ac.uk
www.orc.soton.ac.uk
Phone: +44 23 8059 3101
Fax: +44 23 8059 3142
Mobile: +44 79 5753 6468

known to result in decreased parametric conversion, its influence should be identical on every pulse. This discrepancy may however be explained by the evolution of the relative polarization of the interacting waves. The theoretical work of Lin and Agrawal suggests that polarization mode dispersion (PMD), resulting from birefringence, not only leads to a decrease in the average parametric gain, but also to considerable fluctuations in the generated sidebands [16]. These fluctuations, which were found to scale with the magnitude of the frequency-shift, may therefore be responsible for the pulse-to-pulse variation detected for our OPO. Since the OPO of the current work is significantly different from the generic FWM treated in Ref. [16], a detailed investigation into the influence of polarization in our case should provide further insight. If the parametric gain in our OPO is indeed subject to degradation as a result of polarization effects and longitudinal inhomogeneity along the PCF, it seems conceivable that small contributions over the full PCF length will add up to produce the observed FWM at the wavelengths which have the highest degree of effective phase-matching. The presence of such a distributed gain may thus be an argument for the use of an even longer PCF. Although the use of very long fibers (several times the walk-off length) has not been reported for a PCF-based OPO, Sloanes *et al.* have reported relatively high conversion efficiencies for a PCF-based optical parametric amplifier of this type [17].

All-fiber OPO configurations have been a focus of research for some time now. However, the development of these sources has been limited, almost exclusively, to the 1550 nm spectral region, where established technology such as erbium-doped fiber amplifiers and dispersion-shifted fibers have provided the building blocks [18, 19, 20]. It is therefore our believe that, despite the requirement for numerous improvements, our demonstration of an all-fiber PCF-based OPO cavity represents the first of its kind outside of the established 1550 nm wavelength region. To the best of our knowledge, the achieved pump-to-anti-Stokes conversion efficiency of 8.6% over 142 THz, is the highest fiber OPO conversion efficiency over such a large frequency-shift, to date.

6 Future work

It is clear that the OPO can still be significantly improved. In colaboration with *Shinkosha*, special-purpose fiberized isolators with built-in filters are currently being developed. This component will enable the assembly of a fully fiber-integrated pump-OPO device, which should result in increased mechanical stability and improved pump coupling efficiency. Futhermore, we are also considering different methods to decrease nonlinear effects in the delay fiber. Two options are to decrease the intra-cavity power by increasing the output-coupling ratio, or to employ delay line filtering elements to reduce the build-up of SRS. Ideally, a shorter delay fiber will be implemented, although this will necessitate a higher pump repetition frequency, and consequently a higher pump average power, due to the synchronous pumping arrangement.

The requirement for a shorter delay fiber may well lead to improvements to the MOPA. Currently, we endeavor to replace the ring-laser MOPA seed source with a narrow linewidth single-mode diode. This is expected to increase the overall temporal stability of the MOPA, which may in turn result in better parametric conversion. As polarization instability remains a concern, the intention is to replace the cavity delay fiber, as well as fiber couplers, with PM equivalents. In the long-term, this also holds for the PCF nonlinear converter.

7 Personnel working on the project

Principal investigator: *Prof. Johan Nilsson*
Doctoral student: *Gysbert van der Westhuizen*

8 Publications

Paper has been submitted for review.

Johan Nilsson
ORC, University of Southampton
Southampton, UK
jn@orc.soton.ac.uk
www.orc.soton.ac.uk
Phone: +44 23 8059 3101
Fax: +44 23 8059 3142
Mobile: +44 79 5753 6468

9 Interactions/Transitions

The project participants have had frequent meetings to discuss the progress, typically on a weekly basis. In addition certain technical aspects have been discussed in Southampton with Prof. M. Marhic of the University of Swansea as well as in San Diego with Prof. S. Radic of the University of California, San Diego. Furthermore Dr. Colin McKinstrie of Alcatel-Lucent has kindly helped with certain theoretical aspects, via telephone and email. He has also agreed to help with the analysis of experimental results (yet to be obtained), insofar as he is able to.

Furthermore Johan Nilsson attended a workshop at OFC in San Diego, in February 2008. All of the above-mentioned researchers were present there, together with other leaders in the field.

10 New discoveries, inventions or patent disclosures

None

11 Honors/Awards

None

Johan Nilsson
ORC, University of Southampton
Southampton, UK
jn@orc.soton.ac.uk
www.orc.soton.ac.uk
Phone: +44 23 8059 3101
Fax: +44 23 8059 3142
Mobile: +44 79 5753 6468

References

[1] P.N. Morgan and J.M. Liu, "Parametric four-photon mixing followed by stimulated Raman scattering with optical pulses in birefringent optical fibers," *IEEE Journal of Quantum Electronics*, vol. 27, no. 4, April 1991.

[2] E.A. Golovchenko and A.N. Pilipetskii, "Unified analysis of four-photon mixing, modulation instability, and stimulated Raman scattering under various polarization conditions in fibers," *Journal of the Optical Society of America B*, vol. 11, no. 1, January 1994.

[3] R.H. Stolen and J.E. Bjorkholm, "Parametric Amplification and Frequency Conversion in Optical Fibers," *IEEE Journal of Quantum Electronics*, vol. QE-18, no. 7, July 1982.

[4] M.E. Marhic, K.K.-Y. Wong and L.G. Kazovsky, "Wide-band tuning of the gain spectra of one-pump fiber optical parametric amplifiers," *IEEE Journal of Selected Topics in Quantum Electronics*, vol. 10, no. 5, October 2004.

[5] K.K. Chen, J.H.V. Price, S. Alam, J.R. Hayes, D. Lin, A. Malinowski and D.R. Richardson, "Polarization maintaining 100 W Yb-fiber MOPA producing μJ pulses tunable in duration from 1 to 21 ps," *Optics Express*, vol. 18, no. 14, June 2010.

[6] J.C. Knight, T.A. Birks, P.St.J. Russell and D.M. Atkin, "All-silica single-mode optical fiber with photonic crystal cladding," *Optics Letters*, vol. 21, no. 19, October 1996.

[7] J.D. Harvey, R. Leonhardt, S. Coen, G.K.L. Wong, J.C. Knight, W.J. Whadsworth and P.St.J. Russell, "Scalar modulation instability in the normal dispersion regime by use of a photonic crystal fiber," *Optics Letters*, vol. 28, no. 22, November 2003.

[8] W.J. Wadsworth, N. Joly, J.C. Knight, T.A. Birks, F. Biancalana and P.St.J. Russell, "Supercontinuum and four-wave mixing with Q-switched pulses in endlessly single-mode photonic crystal fibers," *Optics Express*, vol. 12, no. 2, January 2004.

[9] D. Nodop, C. Jauregui, D. Schimpf, J. Limpert and A. Tünnermann, "Efficient high-power generation of visible and mid-infrared light by degenerate four-wave mixing in a large-mode-area photonic crystal fiber," *Optics Letters*, vol. 34, no. 22, November 2009.

[10] L. Lavoute, J.C. Knight, P. Dupriez and W.J. Wadsworth, "High power red and near-IR generation using four wave mixing in all integrated fiber laser systems," *Optics Express*, vol. 18, no. 15, July 2010.

[11] W. Margulis and U. Österberg, "Four-photon fiber laser," *Optics Letters*, vol. 12, no. 7, June 1987.

[12] M.E. Marhic, *Fiber Optical Parametric Amplifiers, Oscillators and Related Devices,* Cambridge University Press, 2008.

[13] K. Cook, C. Xiong and W.J. Wadsworth, "Enhanced four-wave mixing and parametric oscillator in photonic crystal fiber," *Journal of Optics A: Pure and Applied Optics*, vol. 9, October 2007.

[14] G.P. Agrawal, *Nonlinear Fiber Optics,* Third Edition, Academic Press, 2001.

[15] J.S.Y. Chen, S.G. Murdoch, R. Leonhardt and J.D. Harvey, "Effect of dispersion fluctuations on widely tunable optical parametric amplification in photonic crystal fibers," *Optics Express*, vol. 14, no. 20, October 2006.

[16] Q. Lin and G.P. Agrawal, "Effects of polarization-mode dispersion on fiber-based parametric amplification and wavelength conversion," *Optics Letters*, vol. 29, no. 10, May 2004.

[17] T. Sloanes, K. McEwan, B. Lowans and L. Michaille, "Optimization of high average power optical parametric generation using a photonic crystal fiber," *Optics Express*, vol. 16, no. 24, November 2008.

[18] G.K.L. Wong, S.G. Murdoch, R. Leonhardt, J.D. Harvey and V. Marie, "High-conversion-efficiency widely-tunable all-fiber optical parametric oscillator," *Optics Express*, vol. 15, no. 6, March 2007.

[19] Y.Q. Xu, S.G. Murdoch, R. Leonhardt and J.D. Harvey, "Raman-assisted continuous-wave tunable all-fiber optical parametric oscillator," *Journal of the Optical Society of America B*, vol. 26, no. 7, July 2009.

[20] A. Gershikov, E. Shumakher, A. Willinger and G. Eisenstein, "Fiber parametric oscillator for the 2 μm wavelength range based on narrowband optical parametric amplification," *Optics Letters*, vol. 35, no. 19, October 2010.

Johan Nilsson
ORC, University of Southampton
Southampton, UK

jn@orc.soton.ac.uk
www.orc.soton.ac.uk

Phone: +44 23 8059 3101
Fax: +44 23 8059 3142
Mobile: +44 79 5753 6468

Progress Report

Fiber Optical Parametric Oscillator and Amplifier for High Power, High Efficiency Operation at Around 0.8 μm

12 November 2008

Grant: *FA8655-08-1-3013*
Authors: *Professor Johan Nilsson, Gysbert van der Westhuizen*
Address: *Optoelectronics Research Centre, University of Southampton, Southampton SO17 1BJ, UK*

1 Introduction

This report summarizes the work carried out at the Optoelectronics Research Centre over the period October 2007 to November 2008. The project involves the investigation of fiber-optical parametric amplifiers (OPA) and oscillators (OPO). Whereas the majority of work in this area has been conducted in the spectral region about 1550 nm, this project intends to explore the possibility of using ytterbium-doped fiber lasers (YDFL) and amplifiers (YDFA) as pump sources. The aim is to obtain high power, high conversion efficiency devices, emitting at a wavelength of roughly 800 nm with GHz-level linewidth. For reasons of power scalability we shall only consider conventional fibers (as opposed to microstructured fibers). The contents of this report forms the groundwork for experimental investigations of such OPAs, to follow next in the project.

The following section offers a summary of our key findings, whilst the interested reader are referred to Sections 3 through 7 for a more rigorous discussion.

2 Summary of findings

Our findings are primarily based on theoretical investigations, using a mix of experimental and literature parameter values. A key challenge is to obtain phase matching, and we have focused our investigations on two approaches towards achieving this, in two types of fibers. Note that in normal fibers it is not possible to get phase matching around 1 μm for pump and daughter waves in the same mode and polarization.

One approach is to use inter-modal phase matching, between waves propagating in different modes. We investigated this approach in a *Pirelli* Freelight fiber. We did manage to find phase matching options with a refractive index profile based on the one of this fiber. The conversion efficiency can theoretically be as high as 99.9% in the absence of stimulated Raman scattering (SRS). However, because the overlap integrals relevant for the FWM process are much smaller than those for SRS, we expect that SRS will dominate and that the FWM efficiency will be low. Therefore, we did not pursue this option any further, although other fibers, with other refractive index distributions, mode distributions, and inter-modal phase matching options may well be more promising.

The other approach is to use birefringence phase matching in a polarization maintaining (PM) fiber. We investigated this with a PM fiber from *Fujikura*. Theoretically, the FWM conversion efficiency cannot be as high with this approach. Although the conversion efficiency drops to 71%, the overlap integrals are now much higher, i.e., the same as the SRS overlap integrals. Thus, it should now be possible to avoid SRS, despite a drop to $\frac{1}{3}$ of the intrinsic FWM interaction strength with crossed polarizations, relative to the case with parallel polarizations.

We also looked into the linewidth requirements with birefringence phase matching, and the tolerances on the fiber core size. It would be interesting to operate the fiber OPA CW, e.g., with 10 W of power. The fiber lengths required at this power level (of the order of 3 km) results in a narrow acceptance bandwidth as well as extremely tight fiber tolerances. Therefore, we will initially consider pulsed operation. Numerically, we found that pumping with 1 ns, 1 kW pulses offers very attractive features, such as efficient conversion (up to the theoretical maximum) and short fibers (e.g., 2.6 m). The acceptance bandwidth becomes 33.44 GHz, which can be achieved with seeded pulsed MOPA systems. The core size tolerances become roughly 3 nm. It seems realistic to achieve such tolerances in a fiber as short as 2.6 m. Note also that the tolerances regarding core size fluctuations are much tighter than the tolerances on (average) core size, since the latter can be compensated for by tuning the pump wavelength.

We also calculated the tolerances and acceptance bandwidth for inter-modal phase matching with the Freelight-based fiber. Also in this respect, the Freelight-based fiber with inter-modal phase matching was worse than the *Fujikura* panda fiber with birefringence phase-matching.

Based on our findings, we have designed an experiment for a diode-seeded fiber OPA using birefringence phase-matching in the *Fujikura* panda-fiber. The required components have been ordered, and we are currently building the experimental set-up.

3 Technical background

The process of optical parametric amplification in fibers is based on four-wave mixing (FWM). FWM in fibers are governed by the third order susceptibility and involves a nonlinear interaction among four optical waves that satisfy the conservation of energy condition:

$$\omega_1 + \omega_2 = \omega_3 + \omega_4 \tag{1}$$

Here, $\omega_k = 2\pi\nu_k$ is the angular frequency corresponding to the frequency, ν_k, of the k'th wave[1]. Physically, Equation 1 corresponds to a process in which two photons at frequencies ω_1 and ω_2 are annihilated, whilst one photon at a higher frequency (ω_3) and one at a lower frequency (ω_4), with respect to $\omega_c = (\omega_1 + \omega_2)/2$, are created. No significant transfer of energy between the waves will take place, unless the phase matching condition is satisfied:

$$\beta_1 + \beta_2 = \beta_3 + \beta_4 \tag{2}$$

β_k is the mode propagation constant of the wave at frequency ω_k and is related to the effective refractive index, experienced by the mode, through $\beta_k = \tilde{n}_k\omega_k/c$. c is the speed of light in vacuum. In physical terms, the phase matching condition represents the conservation of momentum.

The process of investigating OPAs are essentially two-fold. Firstly, an appropriate mechanism for the evaluation of optical waveguides is needed. The spectral regions in which phase matching is achievable will depend crucially on the nature of the waveguide. It is therefore imperative to be able to evaluate waveguides in terms of their mode propagation constants and associated mode fields. The second part of the investigation of OPAs is focused on finding solutions to the coupled amplitude equations that governs FWM. For the purpose of this report these two parts of the investigation will be treated independently, even though both parts are required for a full understanding of the FWM interaction.

3.1 Investigating optical fiber waveguides

The starting point for any investigation into electromagnetic phenomena is Maxwell's equations. The dielectric material is taken to have a zero current density and electric charge density. For the calculation of the mode propagation constants and the associated mode fields, the material is assumed to be linear. In a linear medium the induced electric polarization is directly proportional to the electric field. For the time being, we also assume that the propagation medium is isotropic (permittivity, $\varepsilon(r)$, is independent of field polarization). Using the resulting form of Maxwell's equations and the constitutive relations, the following equation is obtained for the electric field $\mathbf{E}(r)$:

$$\nabla \times \nabla \times \mathbf{E}(r) = \omega^2\mu_0\varepsilon(r)\mathbf{E}(r) \tag{3}$$

[1] throughout this report, the angular frequency will be referred to simply as the frequency; all references to frequency shifts will however be in Hz and not rad/s

Johan Nilsson
ORC, University of Southampton
Southampton, UK
jn@orc.soton.ac.uk
www.orc.soton.ac.uk
Phone: +44 23 8059 3101
Fax: +44 23 8059 3142
Mobile: +44 77 5298 4173

The constant μ_0 is the vacuum permeability. For a low-loss dielectric medium, the imaginary part of the complex quantity $\varepsilon(r)$, may be neglected. In this case, the real part of the permittivity is related to the medium's refractive index by $\varepsilon(r) = \varepsilon_0 n^2(r)$, where ε_0 is the vacuum permittivity. If we now consider a wave propagating along the optical axis of a lossless, cylindrical waveguide (say z), the field-phasor solution to Equation 3 will have the following form [1]:

$$\mathbf{E}(r) = \mathbf{E}(x, y, z) = \mathbf{E}_0(x, y)e^{-j\beta z} \tag{4}$$

Here, β is the previously introduced mode propagation constant.

Equation 3 accounts for possible spatial variation in the permittivity and therefore describes wave propagation in inhomogeneous media. The refractive index profiles of so-called step-index fibers may be divided into homogeneous zones that may be solved analytically in terms of the well-known Bessel functions. However, for the most general case of commercial fibers that cannot accurately be approximated as step-index fibers, we must make use of a numerical procedure to solve Equation 3. The numerical procedure is provided through the commercial software *COMSOL* [2] and makes use of the finite element method (FEM). The FEM provides us with the mode propagation constants and corresponding mode fields at a single frequency for a given optical fiber.

3.2 Coupled amplitude equations for FWM

The coupled amplitude equations are a set of equations that describe how waves interact with each other in the presence of nonlinearity. The derivation starts from Maxwell's equations and assumes a nonlinear, homogeneous medium (see for instance Marhic [3]). The analysis is restricted to scalar fields by assuming that all fields are linearly polarized and maintain their polarization with propagation along the waveguide.

We are interested in the partially degenerate case where two of the four frequency components are equal and satisfy $2\omega_1 = \omega_3 + \omega_4$. The corresponding phase matching condition is $2\beta_1 = \beta_3 + \beta_4$. Furthermore, the two photons at frequency ω_1 propagate in the same mode and will be associated with a so-called pump wave (p), whilst the high-frequency (ω_3) and low-frequency (ω_4) components are referred to as the anti-Stokes and Stokes waves, respectively. Since we are interested in generating light on the high-frequency side, we shall denote the anti-Stokes wave as the signal (s) and the Stokes wave as the idler (i).

By applying the slowly varying envelope approximation (SVEA), which amounts to the assumption of a quasi-monochromatic optical field, the coupled amplitude equations may be written as:

$$\frac{dA_p}{dz} = \frac{jn_2\omega_p}{c}[f_{pp}|A_p|^2A_p + 2A_p(f_{ps}|A_s|^2 + f_{pi}|A_i|^2) + 2f_{ppsi}A_p^*A_sA_ie^{j\Delta\beta z}] \tag{5}$$

$$\frac{dA_s}{dz} = \frac{jn_2\omega_s}{c}[f_{ss}|A_s|^2A_s + 2A_s(f_{sp}|A_p|^2 + f_{si}|A_i|^2) + f_{sipp}A_i^*(A_p)^2e^{-j\Delta\beta z}] \tag{6}$$

$$\frac{dA_i}{dz} = \frac{jn_2\omega_i}{c}[f_{ii}|A_i|^2A_i + 2A_i(f_{ip}|A_p|^2 + f_{is}|A_s|^2) + f_{ispp}A_s^*(A_p)^2e^{-j\Delta\beta z}] \tag{7}$$

The nonlinear index coefficient is defined as $n_2 = \frac{3}{8n}\mathrm{Re}(\chi^{(3)})$, where $\chi^{(3)}$ was taken as being frequency independent. n_2 is often approximated as a constant for a specific fiber and is a measure of its nonlinearity. The transverse coordinate dependence of the electric field is confined to the constants f_{ij} and f_{ijkl}, known as the overlap integrals. The overlap integrals are defined as:

$$f_{ij} = \frac{\langle|F_i|^2|F_j|^2\rangle}{\langle|F_i|^2\rangle\langle|F_j|^2\rangle} \tag{8}$$

$$f_{ijkl} = \frac{\langle F_i^*F_j^*F_kF_l\rangle}{[\langle|F_i|^2\rangle\langle|F_j|^2\rangle\langle|F_k|^2\rangle\langle|F_l|^2\rangle]^{1/2}} \tag{9}$$

Following the notation of Agrawal [4], angled brackets indicate integration with respect to the x- and y-coordinates. The phase-mismatch is defined as $\Delta\beta = \beta_s + \beta_i - 2\beta_p$.

The first term on the right-hand side of Equations 5 to 7 gives the interaction of each wave with itself. This interaction leads to self-phase modulation (SPM). SPM is the phenomenon whereby an optical wave induces an intensity-dependent nonlinear shift in its own phase. Similarly, the second and third term on the right-hand side of Equations 5 to 7 gives the interaction of each wave with every other optical wave in the medium. The other wave may be at a different frequency, propagate in a different

Johan Nilsson
ORC, University of Southampton
Southampton, UK
jn@orc.soton.ac.uk
www.orc.soton.ac.uk
Phone: +44 23 8059 3101
Fax: +44 23 8059 3142
Mobile: +44 77 5298 4173

transverse mode or propagate in the opposite direction. This interaction leads to a nonlinear phase shift in an optical wave, induced by one or more additional waves. It is referred to as cross-phase modulation (XPM). It should be noted that the phase shift contribution due to XPM has twice the magnitude of the contribution due to SPM (assuming waves of equal intensity). The final term in the coupled amplitude equations represents four-wave mixing (FWM). The FWM term couples the three distinct waves (in the degenerate case) and requires phase matching for significant power transfer to occur.

4 Evaluation of fibers for OPAs

The numerical procedure used to solve for the mode fields and mode propagation constants of a given waveguide (Section 3) does not include the frequency dependence of the refractive index (chromatic dispersion). In the near infrared spectral region, the dispersion for a bulk medium may easily be included through the Sellmeier equation [5]:

$$n^2(\omega) = 1 + \sum_{j=1}^{3} \frac{B_j \lambda^2}{\lambda^2 - \lambda_j^2} \tag{10}$$

The wavelengths, λ_j, are the resonance wavelengths at which the specific medium absorbs light, while the constants, B_j, indicate the strength of each resonance. In addition to the dispersion found in a bulk medium (material dispersion), the dielectric waveguide also contributes to the total dispersion experienced by a propagation mode. This so-called waveguide dispersion differs depending on the mode in which the light propagates and manifests through the frequency dependence of the mode propagation constant ($\beta(\omega)$).

The total dispersion in fibers is historically presented by the dispersion parameter (D). The dispersion parameter is related to the group-velocity dispersion (GVD), both of which are given by:

$$\beta_2 = \frac{d^2\beta}{d\omega^2} = \frac{1}{c}(2\frac{dn_{\text{eff}}}{d\omega} + \omega\frac{d^2 n_{\text{eff}}}{d\omega^2}) \tag{11}$$

$$D = -\frac{2\pi c}{\lambda^2}\beta_2 \tag{12}$$

Here, n_{eff} denotes the effective refractive index. The wavelength at which the dispersion equals zero is called the zero-dispersion wavelength (ZDW). The region for which $D < 0$ is called the normal-dispersion regime. This regime is associated with wavelengths shorter than the ZDW.

In light of the preceding discussion, the phase-mismatch (introduced in Section 3.2) may be decomposed as follows [4]:

$$\Delta\beta = \Delta\beta_M + \Delta\beta_W + \Delta\beta_{NL} \tag{13}$$

$$\approx [n_s\omega_s + n_i\omega_i - 2n_p\omega_p]/c + [\Delta n_s\omega_s + \Delta n_i\omega_i - 2\Delta n_p\omega_p]/c \tag{14}$$

The subscripts M, W and NL refers to the phase-mismatch contribution due to material dispersion, waveguide dispersion and nonlinear refraction (SPM and XPM). We shall initially neglect $\Delta\beta_{NL}$ for the analysis of this section, but it will be re-introduced in Section 5. Apart from neglecting $\Delta\beta_{NL}$, Equation 14 is obtained from Equation 13 by assuming $n_{\text{eff}} = n + \Delta n$, where n is the material refractive index and Δn is the change in n due to waveguiding.

Longitudinal variations in the core radius or refractive index profile (RIP) of a fiber lead to a z-dependent dispersion. The fact that the dispersion is not constant along the fiber means that the phase-mismatch also varies. The end result of longitudinal inhomogeneity of the waveguide is a decrease in the efficiency of the FWM process. It is for this reason that we are primarily interested in commercial fibers, for which the manufacturing process has been perfected, for obtaining phase matching. Sections 4.1 to 4.3 gives an overview of the techniques whereby the different terms in Equation 14 may be balanced so as to achieve phase matching. The applicability of these techniques for phase matching in commercially available fibers are investigated.

4.1 Fundamental-mode phase matching

A number of commercial fibers have been investigated within the project. Among these are the *Sumitomo* highly-nonlinear fiber (HNLF), the *Corning* SMF28 fiber and the Truewave fiber (*Lucent*). For the

Johan Nilsson
ORC, University of Southampton
Southampton, UK
jn@orc.soton.ac.uk
www.orc.soton.ac.uk
Phone: +44 23 8059 3101
Fax: +44 23 8059 3142
Mobile: +44 77 5298 4173

purpose of illustrating the different results that may be obtained we consider the *Pirelli* Freelight fiber.

The RIP of the Freelight fiber (see Figure 1(a)) was measured and used as input parameter to the numerical simulation. Making use of the Sellmeier equation and the appropriate coefficients, we were able to simulate the total dispersion of the Freelight fiber. Figure 1(b) compares the simulated total dispersion to the measured values. The discrepancy at longer wavelengths means that the phase-matched wavelengths may be slightly different than those predicted by the simulation (see below).

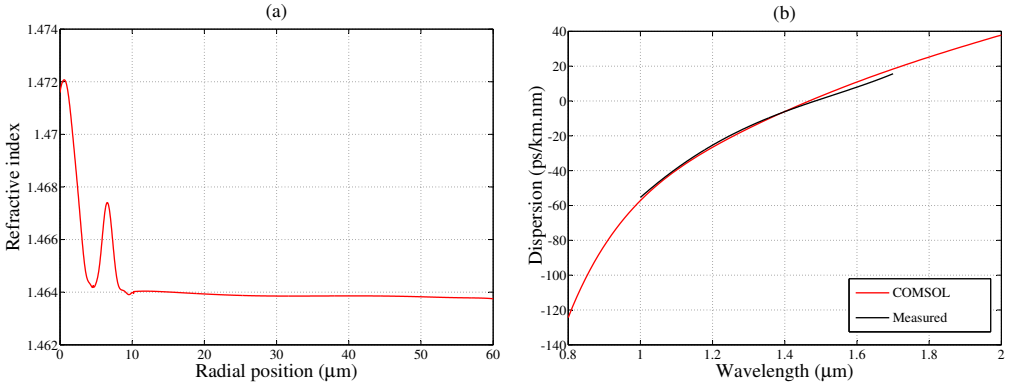

Figure 1: (a) Measured RIP of the Freelight fiber. (b) Comparison between the measured and calculated (*COMSOL*) values for the total dispersion of the Freelight fundamental mode.

The dispersion of the effective refractive index allows us to search for phase-matched components according to $\Delta\beta = \beta_s + \beta_i - 2\beta_p$. This is done by assigning some value to the pump frequency (ω_p), whilst varying the frequency shift ($\Omega = \omega_s - \omega_p = \omega_p - \omega_i$). As Ω is varied, ω_s and ω_i assume specific values which, together with ω_p, satisfies the conservation of energy requirement. The value of n_{eff} at each of the relevant frequencies are obtained through interpolation of the calculated dispersion. The phase-mismatch is calculated before a new value for ω_p is chosen and the process is repeated.

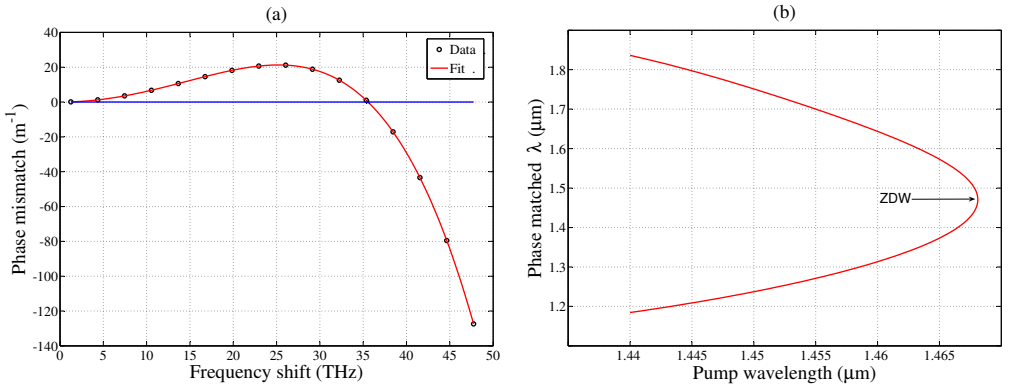

Figure 2: (a) Phase-mismatch at increased values of the frequency shift for $\lambda_p = 1450$ nm and pump, signal and idler in the fundamental mode. (b) Phase matching diagram for the fundamental modes of the Freelight fiber.

The case where all the frequency components are confined to the fundamental mode is considered first. Figure 2(a) gives the result for the Freelight fiber with $\lambda_p = 1450$ nm. A zero phase-mismatch is obtained at a frequency shift of approximately 35.5 THz, which corresponds to a phase-matched signal and idler at $\lambda_s = 1237$ nm and $\lambda_i = 1751$ nm. The ZDW of the Freelight fiber is located at 1468 nm (see Figure 1(b)), which means that the fiber is pumped in the normal dispersion regime. The material contribution to the phase-mismatch is positive below roughly 1316 nm where it reaches the zero material dispersion wavelength and becomes negative thereafter [6][7]. In the normal dispersion regime

Johan Nilsson
ORC, University of Southampton
Southampton, UK
jn@orc.soton.ac.uk
www.orc.soton.ac.uk
Phone: +44 23 8059 3101
Fax: +44 23 8059 3142
Mobile: +44 77 5298 4173

of the fiber, the waveguide contribution to the phase-mismatch is positive when all the frequencies are in the fundamental mode. The effect of the waveguide contribution for pump wavelengths in the range 1316 nm to 1468 nm is therefore to compensate for the material contribution (see Equation 14). From Figure 2 it can be seen that $\Delta\beta_W$ dominates for small frequency shifts and is eventually balanced by the growing negative contribution from $\Delta\beta_M$. The phase matched wavelengths corresponding to the pump wavelengths in the range 1440 nm to 1468 nm is given in Figure 2(b). It is apparent that the frequency shift at which phase matching is obtained decreases as the pump wavelength moves closer to the ZDW. At the ZDW, the frequency shift vanishes yielding the fully degenerate case. Although phase matching can be obtained in the anomalous dispersion regime, it involves the nonlinear contribution to the phase-mismatch and will not be explored here.

The Freelight fiber as well as the other fibers mentioned at the start of Section 4.1 all have a ZDW in excess of 1270 nm, which is the zero material dispersion wavelength for silica. Since we want to pump in the wavelength range 1060 nm to 1080 nm, this method for achieving phase matching is ruled out. When the pump, signal and idler are not confined to the fundamental mode, another method for phase matching becomes available. This method relies on the mode dependence of the waveguide dispersion to tailor the phase-mismatch due to waveguiding (see Equation 14).

4.2 Higher-order mode phase matching

The Freelight fiber supports five modes in the wavelength range 800 nm to 1700 nm, each of which corresponds to a unique cutoff wavelength. From the cutoff wavelengths and the available modes a number of possible mode combinations for phase matching are identified. Among the mode pairs that give phase matching are $\mathrm{LP}^p_{11}\mathrm{LP}^s_{02}\mathrm{LP}^i_{11}$ (for $\lambda_p \leq 1210$ nm), $\mathrm{LP}^p_{02}\mathrm{LP}^s_{21}\mathrm{LP}^i_{02}$ (for $\lambda_p \leq 1010$ nm) and $\mathrm{LP}^p_{02}\mathrm{LP}^s_{21}\mathrm{LP}^i_{11}$ (for $\lambda_p \leq 1130$ nm), where the superscripts indicate the relevant frequency component at every mode. For $\lambda_p = 1060$ nm Figure 3(a) gives the phase matched frequency shift for the $\mathrm{LP}^p_{02}\mathrm{LP}^s_{21}\mathrm{LP}^i_{11}$ combination. As was mentioned in the discussion for the fundamental-mode case, $\Delta\beta_M$ is positive at this wavelength. The specific mode combination however leads to a large negative $\Delta\beta_W$ contribution which is seen to dominate for small frequency shifts before phase matching is obtained at $\Omega/(2\pi) \approx 58$ THz [8][9][10]. Figure 3(b) shows the signal and idler components at the various frequency shifts including the zero-mismatch shift. The dashed lines indicate the cutoff wavelengths for the signal and idler mode and it is clear that both modes are guided at 58 THz. The phase matched wavelengths corresponding to the pump wavelengths in the range 980 nm to 1130 nm is given in Figure 3(c). The trend in the phase matching diagram is noticeably different from that of Figure 2(b) in that the frequency shift for phase matching increases for larger values of λ_p, whilst the two curves also seem to diverge for shorter pump wavelengths.

From Equations 8 and 9 we may now calculate the overlap integrals for the higher-order mode combination of Figure 3. The values of the overlap integrals should reveal the extend to which the respective modes will be able to exchange power. In FWM literature a quantity called the effective area, defined as $A_{\text{eff}} = 1/f$ for f_{ij} or f_{ijkl}, is often used to describe this interaction strength for the processes of SPM, XPM and FWM. The value of A_{eff} is useful since it can be compared to the cross-sectional area of the fiber core. Since the Freelight fiber does not have a well-defined core, we also calculate the overlap integrals (or at least A_{eff}) for the fundamental-mode case of Figure 2 as a reference. Here we are only concerned with the FWM A_{eff}-value which is roughly 40 μm^2 for the fundamental-mode case and approaches infinity for the higher-order mode case. The value of 40 μm^2 makes sense in terms of the dimensions of the Freelight 'core' area, but the higher-order mode value basically indicates zero-overlap. This result makes sense in terms of symmetry considerations and equivalently holds for the other two higher-order mode combinations ($\mathrm{LP}^p_{11}\mathrm{LP}^s_{02}\mathrm{LP}^i_{11}$ and $\mathrm{LP}^p_{02}\mathrm{LP}^s_{21}\mathrm{LP}^i_{02}$). For a LP_{lm} mode the analytical expressions for the mode fields, together with the numerator in Equation 9, may be used to show that one of the following three equations should be satisfied for non-zero overlap [1]:

$$l_s - l_i = 0 \tag{15}$$

$$|l_s - l_i| = 2l_p \tag{16}$$

$$l_s + l_i = 2l_p \tag{17}$$

Analysis of the other fibers mentioned at the start of Section 4.1 shows less higher-order modes than that obtained for the Freelight fiber. This results in a situation where the only possible combination that may be used for phase matching has a zero overlap integral. In order to get an idea of the typical

Johan Nilsson
ORC, University of Southampton
Southampton, UK
jn@orc.soton.ac.uk
www.orc.soton.ac.uk
Phone: +44 23 8059 3101
Fax: +44 23 8059 3142
Mobile: +44 77 5298 4173

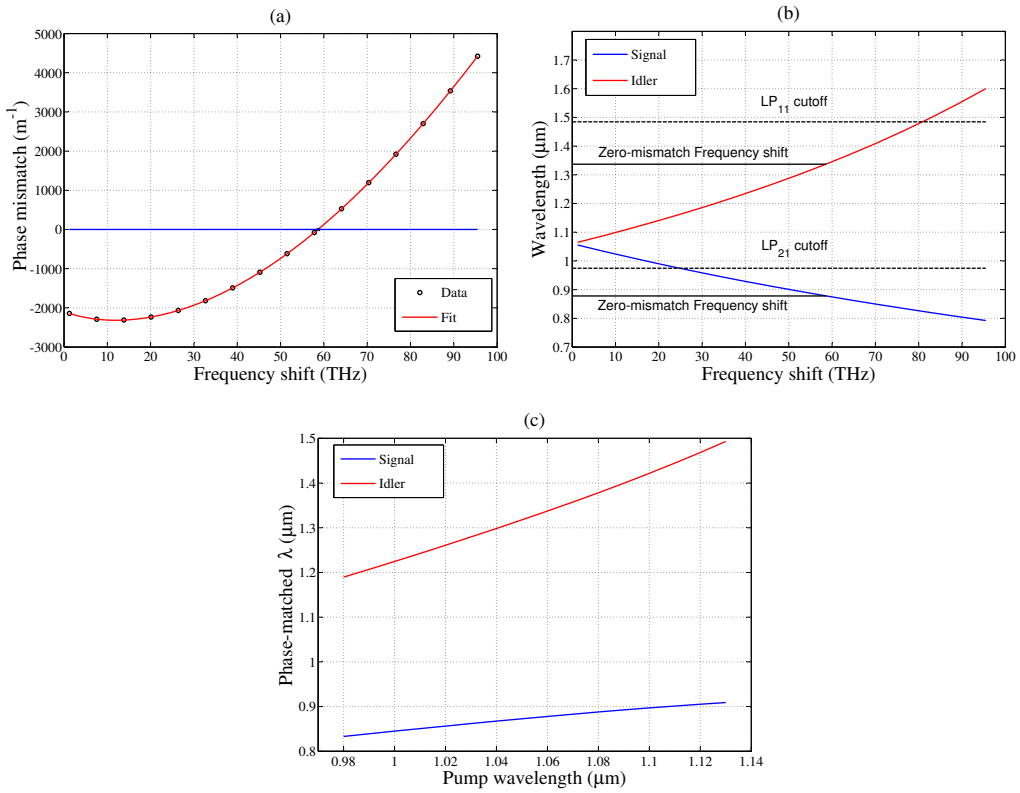

Figure 3: (a) Phase-mismatch for the $LP^p_{02}LP^s_{21}LP^i_{11}$ combination at increased values of the frequency shift at $\lambda_p = 1060$ nm. (b) Cutoff wavelengths for the relevant modes. (c) Phase matching diagram for the combination of higher-order Freelight modes.

A_{eff}-values that can be obtained with this method of phase matching, we decided to customize the RIP of the Freelight fiber. This is done by simply stretching the RIP in the radial direction by a factor ϕ, whilst keeping the cladding size fixed. The value of ϕ can range from 1 to 2, where $\phi = 1$ is the actual dimension for the Freelight fiber. In terms of a step-index fiber this is equivalent to an increase in the core radius. For the purpose of the discussion, this fiber is labeled the 'Adjusted Freelight' fiber.

Similar to the procedure outlined above, the phase-mismatch for various mode combinations is calculated over a range of ϕ-values for a pre-defined frequency shift. This frequency shift is obtained by fixing λ_p to 1060 nm and λ_s to 850 nm and has a magnitude of roughly 70 THz ($\lambda_i = 1408$ nm). A stretch of the RIP not only shifts the cutoff wavelengths of the existing Freelight higher-order modes to longer wavelengths, but also introduces additional guided modes. For this reason, the number of guided modes as well as their cutoff wavelengths have to be identified at every value of ϕ. This gives rise to a potentially large number of mode combinations that may yield phase matching. Most of these mode combinations can however be discriminated against on basis of the modes reaching cutoff and the conditions for non-zero overlap. Among the remaining mode combinations a number of phase matching combinations are identified. The phase-mismatch solution for the case of $\phi = 1.06$, with a mode combination of $LP^p_{02}LP^s_{12}LP^i_{11}$, gives an effective area for FWM of 601 μm^2. This combination therefore offers a feasible method by which phase matching can be achieved for the given spectral range. We shall return to this design in Section 5, where the calculated overlap integrals will be used to obtain solutions to the coupled amplitude equations.

4.3 Birefringence phase matching

A third method whereby phase matching can be obtained makes use of the birefringence in a polarization maintaining (PM) fiber. If a mode is polarized along the x-axis, it will have a different effective refractive index from that of a mode polarized along the y-axis. This means that the effective refractive index

Johan Nilsson
ORC, University of Southampton
Southampton, UK
jn@orc.soton.ac.uk
www.orc.soton.ac.uk
Phone: +44 23 8059 3101
Fax: +44 23 8059 3142
Mobile: +44 77 5298 4173

is not only dependent on the spatial mode of propagation, but also depends on the polarization. Due to this polarization-dependence of a mode's effective refractive index, it is customary to attribute the so-called modal birefringence ($B_m = |\tilde{n}_x - \tilde{n}_y|$) to the waveguide contribution to the phase-mismatch (Equation 14). Thus, instead of using higher-order spatial modes to tailor $\Delta\beta_W$, the polarization modes of the fundamental spatial mode of a fiber may be designed to give specific dispersive behavior [11].

To investigate this method of phase matching we use the *Fujikura* SM98-PS-U25A PM fiber. This fiber uses stress-induced birefringence to maintain the polarization of a mode and is of the panda type. The RIP of the panda fiber along the axis containing the stress-applying parts (SAP) is given in Figure 4(a). The SAPs are indicated by the large area of decreased refractive index (due to the presence of B_2O_3). Orthogonal to the axis shown in Figure 4(a), the RIP looks exactly the same apart from the absence of the SAP (flat cladding). In contrast to the previous simulations, the RIP is approximated by index steps (dashed line). The modal birefringence, B_m, is obtained from a *COMSOL* calculation using the elastic and thermal properties of the fiber materials. In contrast to the fibers considered in Sections 4.1 and 4.2, the equation to be solved for the mode propagation constants and mode fields is the anisotropic equivalent to Equation 3 (due to the refractive index being different for light polarized along the x- and y-direction). The value of $B_m = 4.77 \times 10^{-4}$ at $\lambda = 1000$ nm is in good agreement with that obtained from a measurement of the beat length of this fiber ($B_m = \lambda/L_B = 4.84 \times 10^{-4}$) and also corresponds well to an analytical result, $B_0 = 4.84 \times 10^{-4}$ obtained using the same parameter values [12].

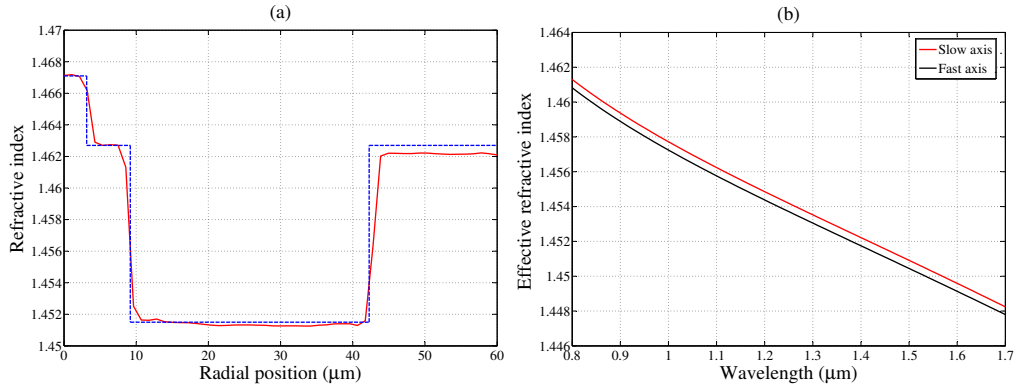

Figure 4: (a) RIP of panda fiber along the axis containing the SAPs. (b) Effective refractive index of the slow- and fast axes, showing the birefringence responsible for maintaining the polarization.

The wavelength dependence of the effective refractive index for the two orthogonal polarization components of the fundamental mode is shown in Figure 4(b). The upper curve, for which the effective refractive index is larger, is denoted the slow axis of the fiber. This is due to the fact that a larger refractive index corresponds to a decrease in the group velocity of light. The modal birefringence shows only a weak dependence on wavelength. From the dispersion characteristics phase matching can be evaluated as before. The positive nature of the $\Delta\beta_M$ contribution to the total phase-mismatch requires a negative contribution from $\Delta\beta_W$, as was the case for the higher-order mode combinations. In the spectral region of interest a negative $\Delta\beta_W$ can be achieved by polarizing the pump wave along the slow axis, whilst the signal- and idler waves are polarized along the fast axes [11]. With $\lambda_p = 1080$ nm, a zero-mismatch is obtained at a frequency shift of 78.5 THz, resulting in phase matched wavelengths at $\lambda_s = 842$ nm and $\lambda_i = 1506$ nm (see Figure 5(a)). As was seen in Figure 3(a), $\Delta\beta_W$ dominates for small frequency shifts before the components eventually balance each other. Figure 5(b) shows that phase matching is furthermore achieved for pump wavelengths ranging from 1040 nm to 1140 nm. Once again, the curves representing the signal- and idler wavelengths appear to diverge to the short- and long wavelength side [13].

The FWM overlap integral for the panda fiber at the specified wavelengths can be solved to give $A_{\text{eff}} = 46\ \mu\text{m}^2$. Although this value is drastically smaller than the value obtained for the Adjusted Freelight fiber ($601\ \mu\text{m}^2$), other differences between the two cases need to be considered before an optimal route can be identified. We shall return to the panda PM fiber in the next section.

Johan Nilsson
ORC, University of Southampton
Southampton, UK
jn@orc.soton.ac.uk
www.orc.soton.ac.uk
Phone: +44 23 8059 3101
Fax: +44 23 8059 3142
Mobile: +44 77 5298 4173

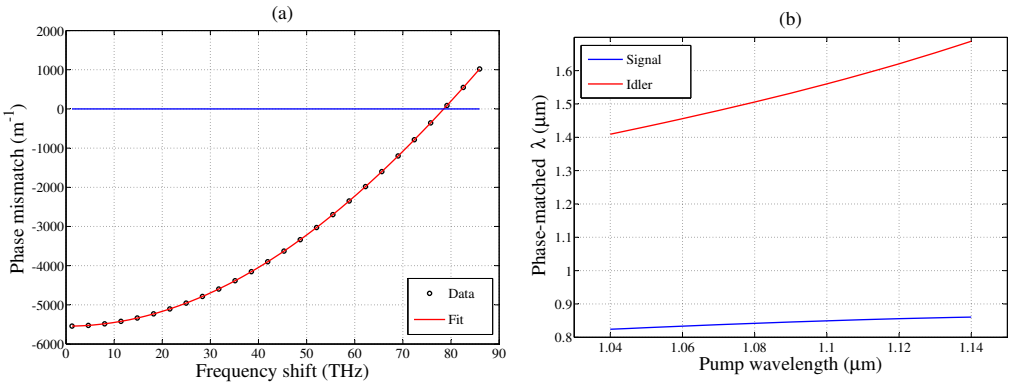

Figure 5: (a) Birefringence phase matching at $\lambda_p = 1080$ nm in a panda fiber. (b) Phase matching diagram for the pump polarized along the slow axis of a panda fiber.

5 Numerical solutions to the coupled amplitude equations

Analytical methods are often used to obtain approximate solutions to Equations 5 to 7. Although these solutions provide physical insight into the workings of the FWM interaction, a numerical procedure is required for a complete description. The contents of this section is based on numerical solutions to the differential equations (DE) of interest. For this purpose we use *MATLAB*'s *ode45* function, which implements a fourth-order Runga-Kutta method to solve the DEs.

At this point it is necessary to motivate the exclusion of stimulated Raman scattering (SRS) and stimulated Brillouin scattering (SBS) from the coupled amplitude equations. Although both of these nonlinear effects involve the interaction of photons with phonons, their behavior and influence on wave propagation differ notably [4]. For a quasi-CW pump or relatively long pulses (> 5 ns), SBS can be mitigated through the use of phase modulation to broaden the pump linewidth [3][14]. Pump pulses shorter than 5 ns (see Section 5.1) are not susceptible to SBS due to their broad linewidths. SRS has a very broad gain spectrum (30 THz with gain peak at roughly 13 THz), as opposed to SBS, and cannot simply be prevented through practical means. In a well-designed FWM experiment where the phase matching condition is satisfied and the FWM effective area is comparable to the fiber core area (Section 4.3), the SRS gain coefficient is up to three times smaller than the parametric gain coefficient. In this case SRS may be neglected as a first approximation [14][15]. This assumption breaks down when the FWM frequency shift is small enough for the idler to spectrally overlap the Raman gain or when the FWM effective area is an order of magnitude larger than the core area (Section 4.2). The effect of SRS may then be incorporated into the coupled amplitude equations by introducing an imaginary part to the third-order susceptibility [3].

For silica fibers the nonlinear index coefficient is assumed to have a constant value of $n_2 = 2.6 \times 10^{-20}$ m$^2/W$ [4]. For typical OPAs the pump power, $P_p = |A_p|^2$, is comparatively large at the input to the fiber, whilst the signal or the idler (or both) are generated from noise. As an approximation to the power contained in the noise at the signal- or idler wavelengths, we use $P_s = P_i = 0.1$ μW [16]. The solutions to the coupled amplitude equations have a periodic nature, with the signal- and idler powers reaching a maximum as the pump power reaches a minimum. This behavior is in agreement with numerical [16] as well as analytical [17][18] solutions from the literature. The sum of the powers at the pump-, signal- and idler wavelength at any propagation distance satisfies the conservation of energy. An increase in the magnitude of the overlap integral values, input pump power or input signal power results in a decrease of the length of fiber required to reach the point of maximum power conversion.

The amplitude at a given wavelength may be expressed as $A_k = \sqrt{P_k}e^{j\theta_k}$, where P_k is the power and θ_k is the corresponding phase. Substituting this expression for the amplitude into Equations 5 to 7, results in the following expression for the exponential in the FWM term [3]:

$$\theta(z) = \Delta\beta z + \theta_s(z) + \theta_i(z) - 2\theta_p(z) \tag{18}$$

The quantity $\theta(z)$ is called the total relative phase of the waves. It can easily be verified that the total relative phase should be zero for maximum power transfer between the pump and the so-called daughter

Johan Nilsson
ORC, University of Southampton
Southampton, UK
jn@orc.soton.ac.uk
www.orc.soton.ac.uk
Phone: +44 23 8059 3101
Fax: +44 23 8059 3142
Mobile: +44 77 5298 4173

waves (signal and idler). The total relative phase is not zero for $\Delta\beta = 0$ as it is defined in Equation 14. This is due to the presence of SPM and XPM, manifesting through the individual phases of the three waves (θ_s, θ_i and θ_p), and is exactly the term neglected from Equation 13 ($\Delta\beta_{NL}$). The influence of SPM and XPM is to shift the optimum phase-mismatch to some negative value (for the case of isotropic fibers). The magnitude of the shift itself depends on the input power. Detuning $\Delta\beta$ from its optimum value for a specific case results in an undepleted pump wave as well as a shift in the fiber length for which the maximum power conversion occurs. This behavior has been studied in the literature and analytical formulations exist [18][19][20]. In general, the initial relative phase also influences the fiber length for which maximum power conversion takes place. This is however not the case when the pump and the signal is injected at the fiber input, with the idler growing from noise [21].

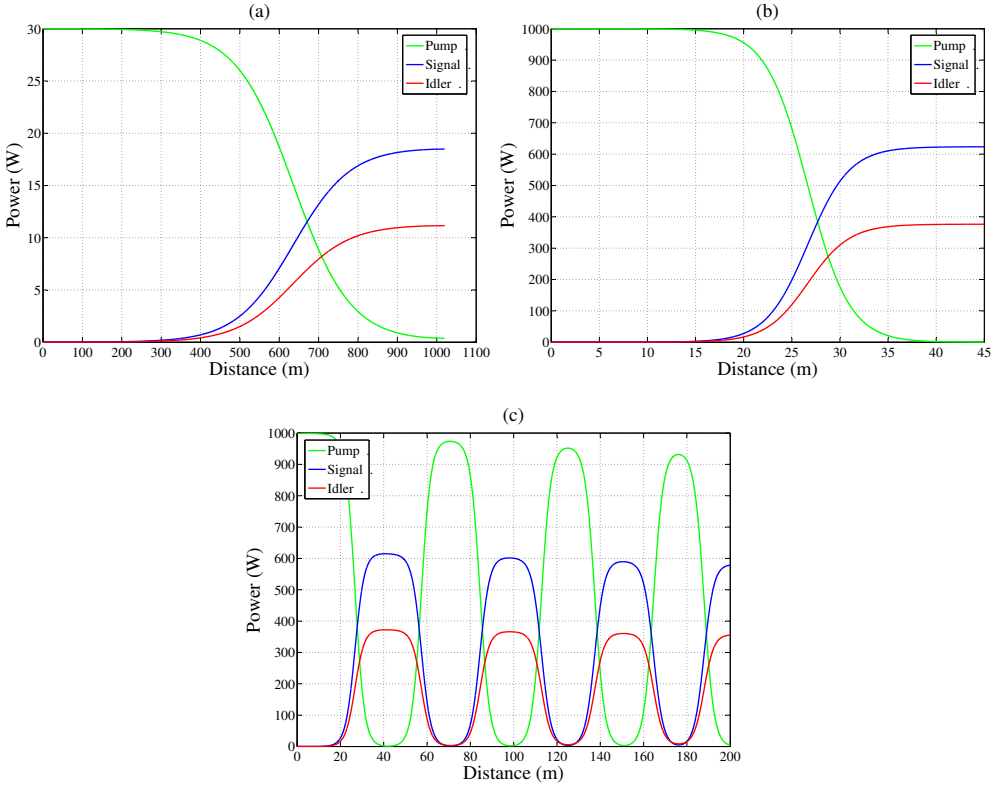

Figure 6: Optimized results for an OPA using the Adjusted Freelight fiber: (a) $P_p = 30$ W (CW pump), (b) $P_p = 1$ kW (pulsed pump), (c) Influence of fiber loss ($P_p = 1$ kW).

5.1 Scalar OPA solutions

We are now in a position to obtain an optimized representation of an OPA constructed from the Adjusted Freelight fiber. Figure 6(a) shows the case with $P_p = 30$ W, $P_s = 10$ mW and a noise-level idler. Using the calculated value for every overlap integral, maximum power conversion is achieved at 1020 m with $\Delta\beta = -0.003$ m^{-1}. The signal experiences a gain of 32.7 dB, whilst the pump-to-signal conversion efficiency is 62%. The example of Figure 6(a) is realistic in terms of a CW pump wave. If we, however, want to increase the pump power to 1 kW, the pump will have to be pulsed. In doing so, the pulse width will have to be long enough to ensure that the assumptions, made during the derivation of the coupled amplitude equations, are not violated. In addition, a square shaped pulse is required in order to keep the peak power and consequently, $\Delta\beta_{NL}$, as constant as possible. An example of a pulsed pump OPA is given by Figure 6(b), where $P_p = 1$ kW and the maximum conversion is achieved at 45 m with $\Delta\beta = -0.104$ m^{-1}. In this case the signal gain is 48 dB. The solution clearly shows the reduction in fiber length that results from using a large pump power. Following on the discussion of Section 4, the use of short fibers are preferred due to the requirement for longitudinal homogeneity.

Johan Nilsson
ORC, University of Southampton
Southampton, UK
jn@orc.soton.ac.uk
www.orc.soton.ac.uk
Phone: +44 23 8059 3101
Fax: +44 23 8059 3142
Mobile: +44 77 5298 4173

The solutions discussed so far have neglected the influence of fiber loss. Loss can, however, be included into the coupled amplitude equations simply by adding a term, $-\frac{\alpha_k}{2}$, to Equations 5 to 7 [3]. Here, α_k is the attenuation constant and has a value of 0.203 km^{-1}, 0.514 km^{-1} and 0.334 km^{-1} at the pump-, signal- and idler wavelength, respectively [22]. The solution to the resulting set of equations are shown in Figure 6(c). Apart from the obvious decrease in power for consecutive maxima of pump, signal and idler, the maxima also experience a shift towards shorter fiber lengths. For the first maximum this is due to attenuation alone, but for the following maxima this shift is a consequence of attenuation as well as incomplete conversion of signal- and idler power back to pump power. This residual power from the preceding cycle shortens the length of fiber required to reach the power maximum in the following cycle. A comparison of Figures 6(b) and (c) shows that loss is effectively responsible for decreasing the maximum signal power after one cycle to 614.8 W (down from 623.4 W). The fiber length corresponding to this maximum is 41 m for the case with loss (down from 45 m). Since this is a fairly small effect we shall, as a first approximation, neglect fiber loss.

5.2 Vector OPA solutions

For a PM fiber with the pump- and daughter waves polarized along the slow- and fast axis, respectively, the scalar coupled amplitude equations need to be adjusted. A vector equivalent to Equations 5 to 7 may be obtained by writing $\vec{A_k} = A_k \hat{e}_k$, where A_k is the scalar amplitude and $\hat{e}_k$ is the normalized Jones vector. By applying a vector operation [3],

$$[\hat{e}_i, \hat{e}_j, \hat{e}_k, \hat{e}_l] = \frac{1}{3}[(\hat{e}_i \cdot \hat{e}_j)(\hat{e}_k \cdot \hat{e}_l) + (\hat{e}_j \cdot \hat{e}_k)(\hat{e}_i \cdot \hat{e}_l) + (\hat{e}_k \cdot \hat{e}_i)(\hat{e}_j \cdot \hat{e}_l)] \tag{19}$$

to the SPM-, XPM- and FWM terms of the described PM fiber, it can be shown that all XPM- and FWM terms, except for the XPM interaction between the signal and idler, are multiplied by a factor of $\frac{1}{3}$. The factor of $\frac{1}{3}$ has its origins in the fact that the perpendicular magnitude of $\chi^{(3)}$ is roughly three times smaller than the parallel magnitude of $\chi^{(3)}$. With these pre-factors, the coupled amplitude equations may be solved as before.

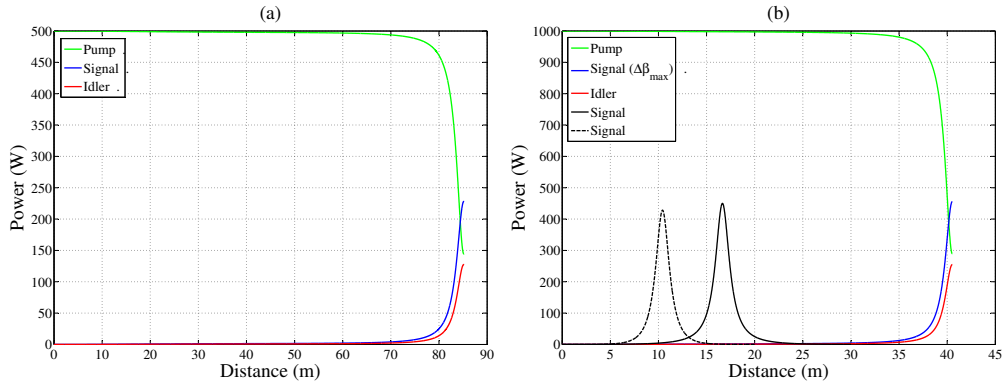

Figure 7: Optimized results for an OPA using the panda PM fiber: (a) $P_p = 500$ W, (b) $P_p = 1$ kW ($\Delta\beta_{NL} =$ 0.249 m^{-1} (blue line), 0.3 m^{-1} (black line) and 0.5 m^{-1}(black dashed line)).

For the evaluation of an OPA constructed from the panda fiber (Section 4.3), we shall focus on the pulsed pump scenario. Figure 7(a) shows the solution obtained from the calculated overlap integral values and $P_p = 500$ W, $P_s = 10$ mW and $P_i = 0.1$ μW. The signal gain reaches a maximum of 44 dB at 85 m for $\Delta\beta = 0.122$ m^{-1}. This maximum power transfer corresponds to a 71% depletion of the pump power and should be compared to the full pump depletion obtained in Section 5.1. In addition to the incomplete power transfer, this result for the panda fiber differs from the results of Section 5.1 in that the optimum value of $\Delta\beta$ is positive. Both these features are characteristic of OPAs based on orthogonal polarizations [14]. The case with $P_p = 1$ kW is given by Figure 7(b). With $\Delta\beta_{\max} = 0.249$ m^{-1} the maximum signal gain of 47 dB is obtained for a fiber length of 40.5 m. For this signal gain the pump-to-signal conversion efficiency is 45%. Also indicated on Figure 7(b) is the signal power for $\Delta\beta$ values of 0.3 m^{-1} (solid line) and 0.5 m^{-1} (dashed line). Although the two larger values for $\Delta\beta$ are detuned from the optimum value and lead to less power transfer, the transfer is achieved at shorter fiber lengths. This

Johan Nilsson
ORC, University of Southampton
Southampton, UK
jn@orc.soton.ac.uk
www.orc.soton.ac.uk
Phone: +44 23 8059 3101
Fax: +44 23 8059 3142
Mobile: +44 77 5298 4173

provides us with the option to tune the phase-mismatch in order to maximize the signal power at the end of a shorter fiber. In fact, at $P_p = 1$ kW, the panda fiber gives parametric gain from $\Delta\beta = 0.2$ m^{-1} to $\Delta\beta = 4.5$ m^{-1}. This range of 4.3 m^{-1} should be compared to the 1.05 m^{-1} range of the Adjusted Freelight fiber. The range over which $\Delta\beta$ can be tuned to give parametric gain is related to the OPA bandwidth.

5.3 Optical parametric oscillators

The OPAs of the preceding sections may be converted into optical parametric oscillators (OPO) through the introduction of feedback. For the case of a linear cavity, this feedback is typically provided by fiber Bragg gratings (FBG). The FBGs are manufactured to reflect a certain percentage of light within a given spectral range. When a pump wave is injected into a linear cavity OPO, the signal and idler are generated from noise. If the cavity is resonant at the signal wavelength, the signal and idler will grow with propagation distance, after which the idler, pump and a fraction of the signal are coupled out of the fiber. The remainder of the signal is reflected and such a cavity is called a bidirectional singly resonant oscillator (SRO) [3]. The bidirectional prefix refers to the counter-propagating signal.

As with any oscillator, the power transfer inside the cavity has a steady state solution. The nature of this steady state solution is influenced by the characteristics of the cavity and will determine the output from the oscillator. In the absence of fiber loss the steady state is obtained once $P_s(L)T = P_s(0)$, with T being the total cavity transmittance [3]. For a cavity with a 100% reflectivity (R_1) on the one end and a 90% relectivity (R_2) on the other, $T = 0.9$. Through an iterative procedure we can calculate the intra-cavity power for the signal that will satisfy the steady state condition for a given pump power and fiber length (L). Strictly speaking, the counter-propagating signal will interact with the co-propagating signal, pump and idler through the processes of SPM and XPM. We shall, however, neglect this for the time being.

The OPO theory, given above, follows on the OPA theory which assumes CW waves. The theory can be applied to pump pulses, giving rise to signal and idler pulses, provided that the pulses do not walk off each other [23]. In this case the pulse repetition period should be matched to the cavity round-trip time of the signal pulse. This will also justify the assumption whereby the SPM and XPM between the co-propagating waves and counter-propagating signal are neglected.

Figure 8(a) and (b) give the results for OPOs, constructed from the panda fiber. The case of (a) corresponds to $P_p = 500$ W and $T = 0.1$ (R_1=100% and R_2=10%) and shows the intra-cavity steady state powers. The maximum transfer occurs for 5.2 m, at the end of the cavity. At steady state $P_s(0) = 24$ W and the signal output from the oscillator is simply $P_s(L)[1 - T] = 217$ W. Similarly, (b) corresponds to $P_p = 1000$ W and the same value for the cavity transmittance. The signal output from the oscillator increases by a factor of two ($P_s(L)[1 - T] = 433$ W), whilst the fiber length for maximum transfer decreases by a factor of two (2.6 m). These short fiber lengths make the OPO configuration an attractive option.

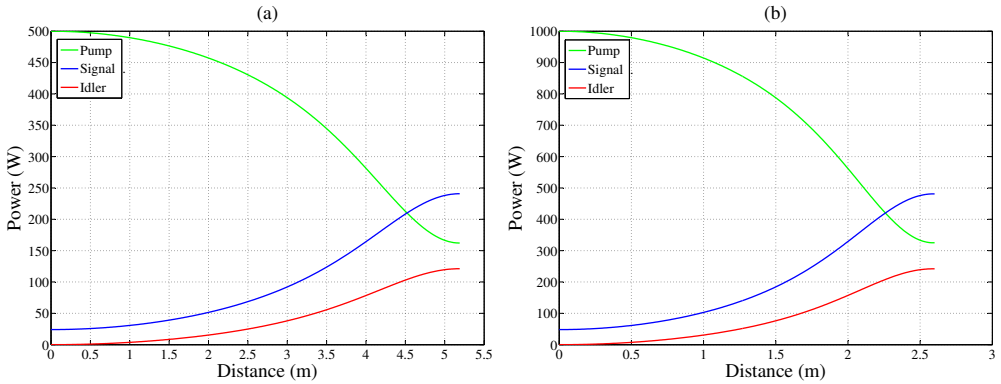

Figure 8: Optimized results for an OPO using the panda PM fiber: (a) $P_p = 500$ W, (b) $P_p = 1$ kW. For both cases $T = 0.1$ is used.

Johan Nilsson
ORC, University of Southampton
Southampton, UK
jn@orc.soton.ac.uk
www.orc.soton.ac.uk
Phone: +44 23 8059 3101
Fax: +44 23 8059 3142
Mobile: +44 77 5298 4173

6 Bandwidth considerations

The analysis of Section 4 culminated in the identification of two possible fibers that may be used for FWM in the spectral region of interest. Despite the fact that the panda fiber has greater mode overlap than the Adjusted Freelight fiber, the use of orthogonal polarizations leads to a decrease in efficiency. The end result of these effects are clear from a comparison of Figures 6(b) and 7(b). The Adjusted Freelight fiber reaches its maximum power conversion after an additional 5 m of propagation, but yields virtually complete pump depletion in comparison to the 71% obtained for the panda fiber. As far as optical parametric amplification is concerned, a crucial difference between the two fibers is the range for which $\Delta\beta$ gives parametric gain (Section 5.2). This range is called the mixing bandwidth ($\Delta\kappa$) and is a function of the pump power as well as the fiber length. The mixing bandwidth is related to the OPA frequency bandwidth by [8],

$$\Delta\Omega = \Delta\kappa \frac{d\Omega}{d(\Delta\beta)}\bigg|_{\Delta\beta=0} \tag{20}$$

where Ω is the frequency shift defined in Section 4.1.

The derivative in Equation 20 can be calculated from an approximate expression for the phase-mismatch, assuming a constant waveguide contribution [8]. The exact value can, however, be calculated from the numerical results. The value is obtained as 7.54×10^9 m/s and, with the use of $\Delta\kappa = 4.3$ m^{-1}, the OPA frequency bandwidth is 32.44 GHz at a pump power of 1 kW.

With the calculated frequency bandwidth, we are now in a position to estimate the amount of core-size variation that can be tolerated whilst still yielding parametric gain. This is done by increasing the core radius of the panda fiber by 1% and calculating the resultant phase matching for $\lambda_p = 1080$ nm. The magnitude of the modal birefringence is found to be invariant to this small increase in the core radius, in agreement with analytical expressions used for the calculation of the birefringence [12]. The zero-mismatch frequency shift (Ω_0) corresponding to the 1% increase is 245.6 GHz larger than that of the initially calculated value for Ω_0. Assuming a linear relation between the magnitude of the core radius variation and the increase in the zero-mismatch frequency shift, it is clear that core radius variations in excess of roughly 0.1% (≈ 0.003 μm) will decrease the gain. Physically, the core radius variation shifts the generated signal- and idler waves out of the gain bandwidth. Although the signal- and idler waves still experience gain at the shifted wavelengths, the overall power transfer to the calculated wavelengths of Section 4.3 deteriorates. This dependence of the overall power transfer on the longitudinal homogeneity of the fiber may well lead to very different behavior than that indicated in the figures of Section 5. An additional requirement for high gain is to have a pump linewidth less than the parametric gain bandwidth. These are all issues that will be addressed in the next step of the project.

Due to the strict bandwidth and longitudinal homogeneity requirements for the build-up of signal- and idler power, the panda fiber seems to be the more appropriate choice for the construction of an OPA or OPO. Although this fiber will require precision control of the polarization at all times, the Adjusted Freelight fiber has more complications. The Adjusted Freelight fiber will have to be manufactured to a high precision after which the quality of the power transfer will still depend crucially on the extent to which bending loss in the fiber influences the higher-order modes. Due to the Adjusted Freelight fiber's large FWM effective area, SRS may well dominate the parametric gain. Further simulations including the effect of SRS may be necessary if we are to consider the Adjusted Freelight fiber as a means for phase matching.

7 Future work

Current work involves the construction of an experimental setup for a PM OPA. Figure 9 gives a diagrammatic representation of what the completed setup will look like. The setup consists of three main sub-assemblies, namely a tunable YDFL source, multiple YDFA stages and the nonlinear (NL) converter. As a NL converter we shall use the panda fiber for the reasons outlined in Section 6. This means that all the fiberized components (circulator, output coupler (OC), tap couplers (TAP), isolator, electro-optic modulator (EOM), wavelength division multiplexer (WDM), tapered fiber bundles (TFB) and Anti-Stokes seed) as well as the double-clad ytterbium-doped fiber, used in the YDFL and YDFAs, must be PM.

Johan Nilsson
ORC, University of Southampton
Southampton, UK
jn@orc.soton.ac.uk
www.orc.soton.ac.uk
Phone: +44 23 8059 3101
Fax: +44 23 8059 3142
Mobile: +44 77 5298 4173

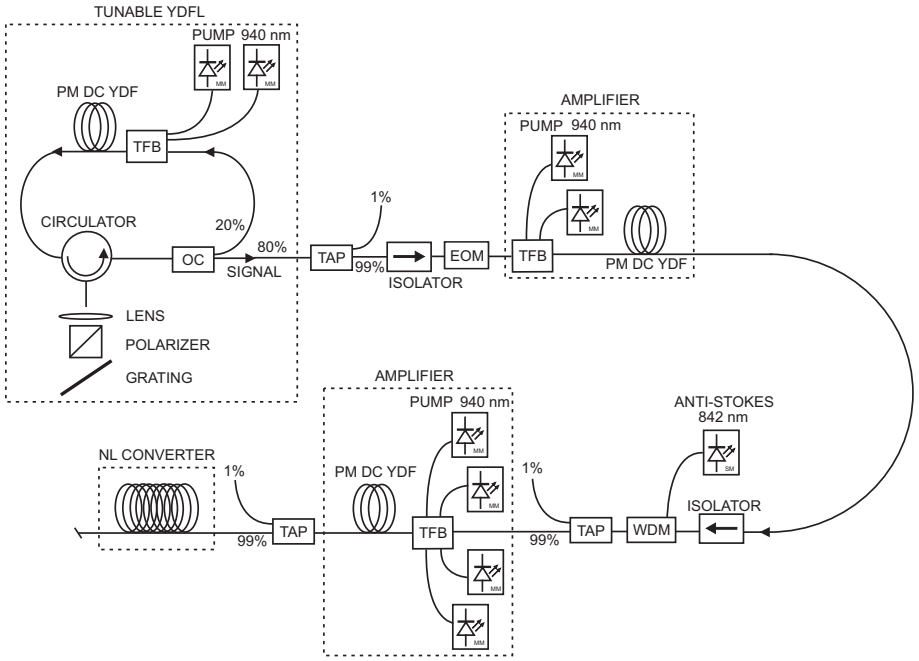

Figure 9: Experimental setup for a PM OPA. Tunable CW output from the YDFL (1080 nm) is modulated by an electro-optic modulator (EOM). A wavelength division multiplexer (WDM) enables the co-propagation of the Anti-Stokes wave (842 nm) and the amplified OPA pump pulses.

The tunable output from the YDFL (1080 nm) will enable us to search for the signal and idler wavelengths corresponding to maximum FWM gain. This alleviates the precision required from the design presented in this report. The tap couplers are simply there to monitor the OPA pump power throughout the setup. High-power isolators are used to prevent possible back-reflections from damaging low-power components. Since the use of pump pulses are required in order to reach the peak powers discussed in Sections 5.2 and 5.3, the CW output from the amplifier needs to be modulated. For this purpose an EOM will be used. The Anti-Stokes wave (signal) at 842 nm is provided by a single-mode (SM) diode laser and is coupled into the OPA pump fiber through a WDM. Alternatively, the Stokes wave (idler) can be used to seed the OPA. An attraction of seeding at the idler wavelength is the fact that tunable laser sources are available in this spectral region (1506 nm). At the output from the panda NL converter, the three wavelength components can be separated by dichroic mirrors. Apart from the bulk components required for the tuning of the YDFL (which can also be fiberized if necessary), the all-fiber setup of Figure 9 should scale well in power.

Depending on initial results, the OPA experimental setup can be converted into an OPO setup with minimum effort. The OPO setup is given in Figure 10 and is identical to that of the OPA, except for the absence of a signal or idler wave input and the presence of the FBGs about the NL converter. The FBG at the input to the NL converter is highly transmittive (HT) at the pump wavelength, whilst it is highly reflective (HR) at the signal wavelength. Similarly, the FBG at the output is highly transmittive (HT) at the pump and idler wavelengths, whilst 90% of the signal is transmitted. The uncertainty in the exact signal and idler wavelengths for which the FWM gain will be a maximum provides the incentive for initial experiments in the OPA configuration. The OPA experiments will identify the exact wavelengths for which the FBGs should be manufactured.

Johan Nilsson
ORC, University of Southampton
Southampton, UK
jn@orc.soton.ac.uk
www.orc.soton.ac.uk
Phone: +44 23 8059 3101
Fax: +44 23 8059 3142
Mobile: +44 77 5298 4173

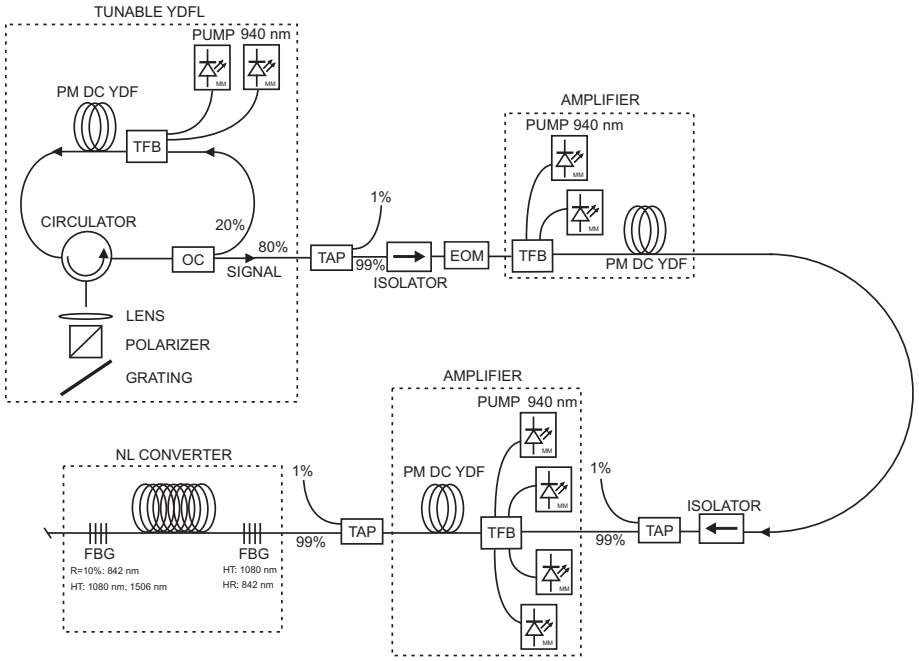

Figure 10: Experimental setup for a PM OPO. Setup is similar to that of the OPA, except for the absence of a signal or idler wave input and the presence of the FBGs about the NL converter. HT denotes highly transmittive and HR highly reflective.

8 Personnel working on the project

Principal investigator: *Prof. Johan Nilsson*
Research staff: *Dr. Jean-Noel Maran*
Doctoral student: *Gysbert van der Westhuizen*

9 Publications

None

10 Interactions/Transitions

The project participants have had frequent meetings to discuss the progress, typically on a weekly basis. In addition certain technical aspects have been discussed in Southampton with Prof. M. Marhic of the University of Swansea as well as in San Diego with Prof. S. Radic of the University of California, San Diego. Furthermore Dr. Colin McKinstrie of Alcatel-Lucent has kindly helped with certain theoretical aspects, via telephone and email. He has also agreed to help with the analysis of experimental results (yet to be obtained), insofar as he is able to.

Furthermore Johan Nilsson attended a workshop at OFC in San Diego, in February 2008. All of the above-mentioned researchers were present there, together with other leaders in the field.

11 New discoveries, inventions or patent disclosures

None

Johan Nilsson
ORC, University of Southampton
Southampton, UK
jn@orc.soton.ac.uk
www.orc.soton.ac.uk
Phone: +44 23 8059 3101
Fax: +44 23 8059 3142
Mobile: +44 77 5298 4173

12 Honors/Awards

None

Johan Nilsson
ORC, University of Southampton
Southampton, UK
jn@orc.soton.ac.uk
www.orc.soton.ac.uk
Phone: +44 23 8059 3101
Fax: +44 23 8059 3142
Mobile: +44 77 5298 4173

References

[1] J.A. Buck, *Fundamentals of Optical Fibers,* John Wiley and Sons, Inc., 1995.

[2] COMSOL Multiphysics, *RF Module User's Guide,* Copyright 1994-2007.

[3] M.E. Marhic, *Fiber Optical Parametric Amplifiers, Oscillators and Related Devices,* Cambridge University Press, 2008.

[4] G.P. Agrawal, *Nonlinear Fiber Optics,* Third Edition, Academic Press, 2001.

[5] J.W. Fleming, "Material Dispersion in Lightguide Glasses," *Electronics Letters*, vol. 14, no. 11, April 1978.

[6] C. Lin, W.A. Reed, A.D. Pearson and H.-T. Shang, "Phase matching in the minimum-chromatic-dispersion region of single-mode fibers for stimulated four-photon mixing," *Optics Letters*, vol. 6, no. 10, October 1981.

[7] C. Lin, W.A. Reed, A.D. Pearson, H.-T. Shang and P.F. Glodis, "Designing single-mode fibers for near-IR (1.1-1.7 μm) frequency generation by phase-matched four-photon mixing in the minimum chromatic dispersion region," *Electronics Letters*, vol. 18, no. 2, January 1982.

[8] R.H. Stolen and J.E. Bjorkholm, "Parametric Amplification and Frequency Conversion in Optical Fibers," *IEEE Journal of Quantum Electronics*, vol. QE-18, no. 7, July 1982.

[9] R.H. Stolen, "Phase-Matched-Stimulated Four-Photon Mixing in Silica-Fiber Waveguides," *IEEE Journal of Quantum Electronics*, vol. QE-11, no. 3, March 1975.

[10] C. Lin and M.A. Bösch, "Large-Stokes-Shift stimulated four-photon mixing in optical fibers," *Applied Physics Letters*, vol. 38, no. 7, April 1981.

[11] R.H. Stolen, M.A. Bösch and C. Lin, "Phase matching in birefringent fibers," *Optics Letters*, vol. 6, no. 5, May 1981.

[12] P.L. Chu and R.A. Sammut, "Analytical Method for Calculation of Stresses and Material Birefringence in Polarization-Maintaining Optical Fiber," *Journal of Lightwave Technology*, vol. LT-2, no. 5, October 1984.

[13] E.A. Golovchenko and A.N. Pilipetskii, "Unified analysis of four-photon mixing, modulation instability, and stimulated Raman scattering under various polarization conditions in fibers," *Journal of the Optical Society of America B*, vol. 11, no. 1, January 1994.

[14] M.E. Marhic, K.K.Y. Wong and L.G. Kazovsky, "Fiber optical parametric amplifiers with linearly or circularly polarized waves," *Journal of the Optical Society of America B*, vol. 20, no. 12, December 2003.

[15] Y. Chen, "Combined processes of stimulated Raman scattering and four-wave mixing in optical fibers," *Journal of the Optical Society of America B*, vol. 7, no. 1, January 1990.

[16] A. Vatarescu, "Light Conversion in Nonlinear Monomode Optical Fibers," *Journal of Lightwave Technology*, vol. LT-5, no. 12, December 1987.

[17] Y. Chen and A.W. Snyder, "Four-photon parametric mixing in optical fibers: effect of pump depletion," *Optics Letters*, vol. 14, no. 1, January 1989.

[18] C.J. McKinstrie, G.G. Luther and S.H. Batha, "Signal enhancement in collinear four-wave mixing," *Journal of the Optical Society of America B*, vol. 7, no. 3, March 1990.

[19] S.J. Garth, "Small-frequency-shift stimulated-four-photon mixing in optical fibers: optimum phase-matching conditions," *Applied Optics*, vol. 31, no. 6, February 1992.

[20] G. Cappellini and S. Trillo, "Third-order three-wave mixing in single-mode fibers: exact solutions and spatial instability effects," *Journal of the Optical Society of America B*, vol. 8, no. 4, April 1991.

[21] M.E. Marhic, K.K.-Y. Wong, M.C. Ho and L.G. Kazovsky, "92% pump depletion in a continuous-wave one-pump fiber optical parametric amplifier," *Optics Letters*, vol. 26, no. 9, May 2001.

[22] M. Nakazawa and M. Tokuda, "Measurement of the fiber loss spectrum using fiber Raman optical-time-domain reflectometry," *Applied Optics*, vol. 22, no. 12, June 1983.

[23] D.K. Serkland and P. Kumar, "Tunable fiber-optic parametric oscillator," *Optics Letters*, vol. 24, no. 2, January 1999.

Johan Nilsson
ORC, University of Southampton
Southampton, UK
jn@orc.soton.ac.uk
www.orc.soton.ac.uk
Phone: +44 23 8059 3101
Fax: +44 23 8059 3142
Mobile: +44 77 5298 4173